Bulletin of the Seismological Society of America, Vol. 97, No. 1A, pp. S249–S270, January 2007, doi: 10.1785/0120050619

# Implications of the 26 December 2004 Sumatra–Andaman Earthquake on Tsunami Forecast and Assessment Models for Great Subduction-Zone Earthquakes

by Eric L. Geist, Vasily V. Titov, Diego Arcas, Fred F. Pollitz, and Susan L. Bilek

Abstract Results from different tsunami forecasting and hazard assessment models are compared with observed tsunami wave heights from the 26 December 2004 Indian Ocean tsunami. Forecast models are based on initial earthquake information and are used to estimate tsunami wave heights during propagation. An empirical forecast relationship based only on seismic moment provides a close estimate to the observed mean regional and maximum local tsunami runup heights for the 2004 Indian Ocean tsunami but underestimates mean regional tsunami heights at azimuths in line with the tsunami beaming pattern (e.g., Sri Lanka, Thailand). Standard forecast models developed from subfault discretization of earthquake rupture, in which deep-ocean sea level observations are used to constrain slip, are also tested. Forecast models of this type use tsunami time-series measurements at points in the deep ocean. As a proxy for the 2004 Indian Ocean tsunami, a transect of deep-ocean tsunami amplitudes recorded by satellite altimetry is used to constrain slip along four subfaults of the $M > 9$ Sumatra–Andaman earthquake. This proxy model performs well in comparison to observed tsunami wave heights, travel times, and inundation patterns at Banda Aceh. Hypothetical tsunami hazard assessments models based on end-member estimates for average slip and rupture length ($M_w$ 9.0–9.3) are compared with tsunami observations. Using average slip (low end member) and rupture length (high end member) ($M_w$ 9.14) consistent with many seismic, geodetic, and tsunami inversions adequately estimates tsunami runup in most regions, except the extreme runup in the western Aceh province. The high slip that occurred in the southern part of the rupture zone linked to runup in this location is a larger fluctuation than expected from standard stochastic slip models. In addition, excess moment release (~9%) deduced from geodetic studies in comparison to seismic moment estimates may generate additional tsunami energy, if the exponential time constant of slip is less than approximately 1 hr. Overall, there is significant variation in assessed runup heights caused by quantifiable uncertainty in both first-order source parameters (e.g., rupture length, slip-length scaling) and spatiotemporal complexity of earthquake rupture.

## Introduction

The 26 December 2004 Sumatra–Andaman earthquake was the first $M > 9$ event to be recorded by a global network of broadband seismic stations and regional Global Positioning System (GPS) networks. Analysis of this data has led to a new understanding of the mechanics of great subduction zone earthquakes. In addition, tsunami data from both conventional measurements (postevent surveys and tide gauges) as well as deep-ocean amplitudes recorded clearly for the first time by satellite altimetry, provide the necessary information to reconstruct the evolution of the Indian Ocean tsunami (Titov *et al.*, 2005b; Hirata *et al.*, 2006; Fujii and Satake, 2007). We can use this new knowledge to test existing tsunami forecast and assessment models and determine whether specific improvements are needed when applied to $M > 9$ earthquakes. As tsunami systems are expanded around the world in the aftermath of the 2004 Indian Ocean tsunami, it is important to refine these models for the dual purpose of mitigating future tsunami hazards and reducing false alarms.

Kinematic rupture models for the 2004 Sumatra–Andaman earthquake exhibit complexity on broadscales in both space and time (Ammon *et al.*, 2005). In contrast to smaller events for which tsunami generation can be ade-

quately approximated by instantaneous finite dislocations, the large-scale complexity associated with great earthquakes has a significant effect on tsunami generation in predicting local and regional tsunami waveforms. In the past, seismic inversions for subduction zone earthquakes provided sufficient information for determining tsunami generation (e.g., Geist and Bilek, 2001). For the 2004 Sumatra–Andaman earthquake, however, seismic inversions have been complicated by overlapping seismic phases and have been difficult to perform (Ammon *et al.*, 2005). Analysis of geodetic measurements in combination with seismic inversions, however, have helped to reduce the discrepancy between seismic and tsunami models of the earthquake (Banerjee *et al.*, 2007; Chlieh *et al.*, 2007).

The primary objective of this study is to examine tsunami generation from the 2004 Sumatra–Andaman earthquake at different levels of parameterization for the purpose of forecasting and assessing future tsunamis. Starting from a point-source, scalar representation of the earthquake, we examine what level of information can be obtained about tsunami generation. There are two distinct applications for such an analysis. The first is real-time forecasting as part of a tsunami warning system (Titov *et al.*, 2005a), termed here as forecast models. In this case, tsunami modeling begins with a limited amount of initial information on earthquake rupture (typically moment magnitude and hypocentral location) soon after the event occurs. The second application is hazard assessment, in the form of inundation maps that use either a maximum credible source (Tinti and Armigliato, 2003; González *et al.*, 2005) or a probabilistic assessment that includes all relevant sources and associated uncertainty (Rikitake and Aida, 1988; Ward, 2002; Geist and Parsons, 2006). We call this latter application *assessment models.*

In addition to how tsunami generation models are applied, the necessary level of parameterization is also linked to the propagation distance away from the source. For all but the largest earthquakes, the tsunami wave field can be estimated in the far field using point source or line source descriptions (Ward, 1980, 1982a; Okal, 1988; Pelayo and Wiens, 1992). Geometric spreading of the tsunami tends to smooth out source-related variations in the wave field. However, it is quite clear that slip heterogeneity for great earthquakes can be ascertained from regional and far-field waveforms, as indicated by numerous tsunami inversion studies (e.g., Satake and Kanamori, 1991; Satake, 2002). Thus, whether or not a simple parameterization can be used depends on both the size of the earthquake and the propagation distance. Most of the damaged regions in the Indian Ocean following the 2004 Sumatra–Andaman earthquake occurred at regional, rather than far-field, distances. In this study, we focus on the effects source parameterization has on tsunami amplitudes at regional distances (up to 1500 km) and near the source. These results will have particular application in assessing tsunami hazards for other vulnerable regions such as the Caribbean and Mediterranean where tsunamis can have significant impact at similar distances.

## Background

### Tectonics

The 2004 Sumatra–Andaman earthquake occurred along the interplate thrust separating the oceanic India plate from the overriding Burma (Andaman) microplate that borders the larger Sunda plate (Fig. 1). The convergence direction along this northern part of the Sumatra subduction zone is highly oblique and can be considered a type area for slip partitioning as originally described by Fitch (1972) and later refined in this region by others (Moore *et al.*, 1980; McCaffrey, 1991; Dasgupta and Mukhopadhyay, 1993; McCaffrey *et al.*, 2000). Whereas relative plate convergence is accommodated along the interplate thrust, most of the arc-parallel component of motion is accommodated by the Sumatran strike-slip fault, which trends northward into the Andaman Sea spreading centers (Mukhopadhyay, 1984; Maung, 1987; Bird, 2003). Some of the arc-parallel motion is also accommodated in the forearc region (Genrich *et al.*, 2000), as would be predicted from continuum deformation models (McCaffrey *et al.*, 2000). In addition to an increase in the obliquity of convergence from south to north, there is also a significant increase in the thickness of sediment entering the subduction zone (possibly with a concomitant increase in pore pressure) (Karig *et al.*, 1980; Moore *et al.*, 1980; Prawirodirdjo *et al.*, 1997), a decrease in the width of the forearc (Moore *et al.*, 1980), and a decrease in both the dip and depth of Benioff-zone seismicity (Newcomb and McCann, 1987; Gudmundsson and Sambridge, 1998). Both Moore *et al.* (1980) and Mukhopadhyay (1984) note extensional deformation in the oceanic India plate and downdip tension stress axes for slab earthquakes, respectively, in the Andaman Islands region. Dasgupta and Mukhopadhyay (1993) indicate that the Benioff zone is contorted in the far-northern part of the Sumatra–Andaman subduction zone, and suggest that the India plate and Burma microplate are weakly coupled in this region.

Analysis of (GPS) data indicates that the total relative plate motion between the India and Sunda plates is approximately 45–52 mm/yr (Simons *et al.*, 1999), whereas only about 7–14 mm/yr of convergence is estimated at the latitude of Port Blair, in the Andaman Islands (Paul *et al.*, 2000; Michel *et al.*, 2001). As recurrence times are linked to fault slip rates (Ward, 1994; McCaffrey, 1997; Kagan, 2002), occurrence of great earthquakes along the northern section of the Sumatra–Andaman subduction zone were prone to under sampling by the historic catalog. One of the lessons from this earthquake is that all subduction zones, no matter their convergence rate, should be considered dangerous in terms of producing earthquakes of tsunamigenic magnitude (Bird and Kagan, 2004). Indeed, the Sumatra–Andaman subduction zone had produced a tsunamigenic earthquake in 1881 near the island of Car Nicobar (Ortiz and Bilham, 2003), although prior to the December 2004 earthquake, it was generally unclear whether $M > 9$ earthquakes could occur in highly oblique subduction zones such as this one.

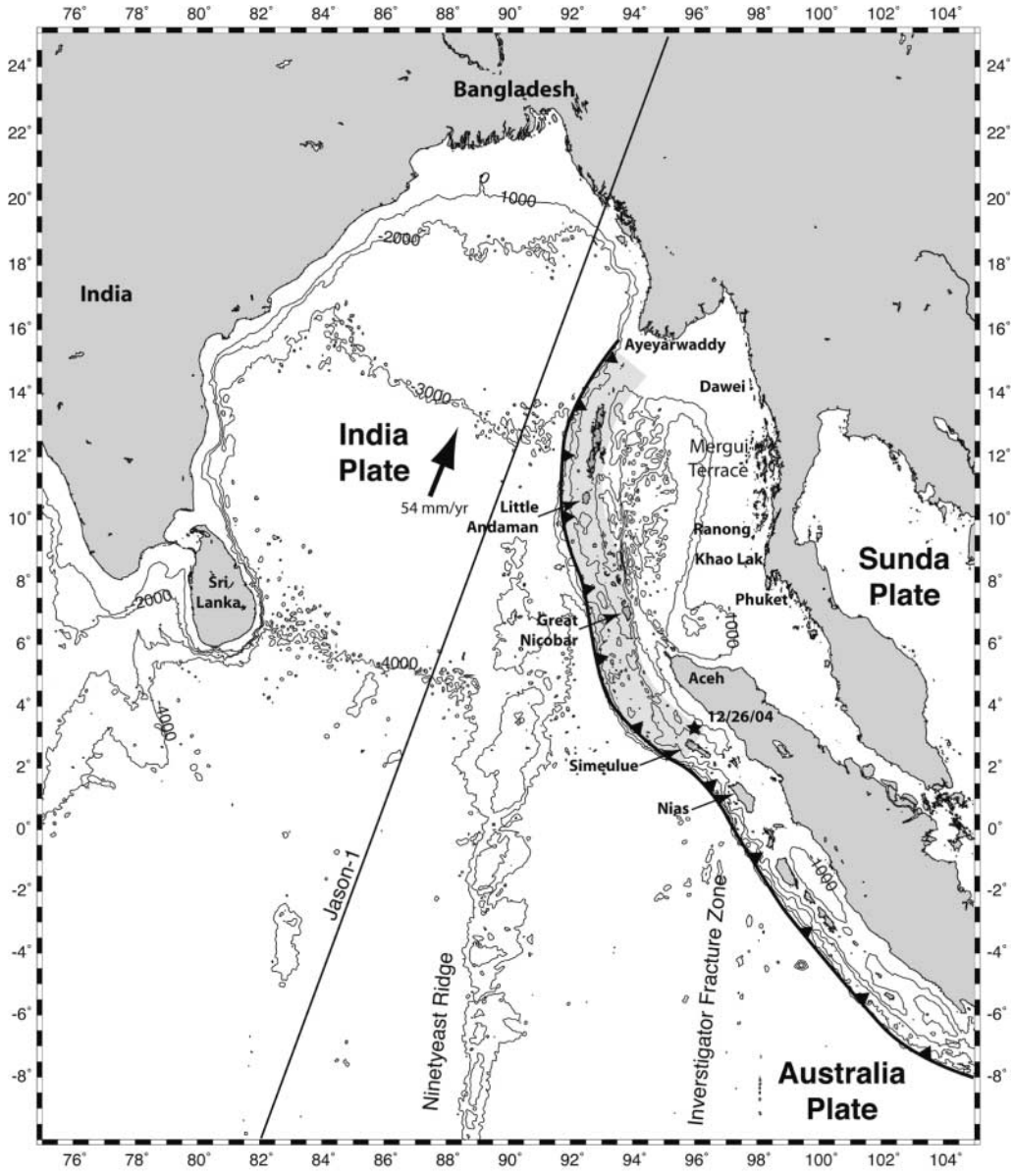


Figure 1. Location map of the study region. Solid line indicates the trackline of the Jason-1 altimetry satellite approximately 2 hr after the 26 December 2004 earthquake (star, epicenter). Shaded region indicates subduction zone segment for which tsunami forecast and assessment models are tested. Sumatra–Andaman interplate thrust indicated by barbed line. Arrow indicates relative motion of the India plate with respect to the Eurasia plate reference frame (Paul *et al.*, 2000). Bathymetric contour interval: 1000 m.

One cannot ignore possible tectonic or geologic controls on rupture for this earthquake. Previous studies have suggested that topographic features of the downgoing plate such as the Ninetyeast Ridge and Investigator Fracture Zone (Fig. 1) are linked to variations in deformation patterns in the overriding plate (Newcomb and McCann, 1987; Dasgupta and Mukhopadhyay, 1993; Krishna and Sanu, 2002). The 2004 earthquake originated near a sharp bend in the trench and a corresponding bend in the subducted slab (Fauzi *et al.*, 1996). Also at this latitude, paleoseismic evidence suggest that this might be a segment boundary for interplate thrust earthquakes—the Simeulue saddle (Sieh *et al.*, 2005).

## Rupture Process for the 2004 Sumatra–Andaman Earthquake

The hypocenter for the December 2004 Sumatra–Andaman earthquake is located just north of Simeulue Island at a depth of 30 km, where rupture propagated unilaterally to the north for approximately 1300–1600 km (Ishii *et al.*,

2005; Lay *et al.*, 2005; Subarya *et al.*, 2006) (Fig. 1). The propagation speed of the rupture front is estimated to be 2.1–2.8 km/sec from imaging using the Hi-Net seismic array in Japan (Ishii *et al.*, 2005) and hydroacoustic data (Tolstoy and Bohnenstiehl, 2005), although de Groot-Hedlin (2005) suggests that the rupture front slowed to about 1.5 km/sec 600 km away from the epicenter. Slower rupture velocities are also suggested by some tsunami studies (Hirata *et al.*, 2006; Fujii and Satake, 2007). As indicated by Ni *et al.* (2005) the high-frequency seismic waves used to image the propagation of the rupture front cannot uniquely map the slip evolution and distribution on the fault. For this, long-period seismic waves were analyzed.

Though the inversions of body and long-period surface waves that have been performed to date differ in specific aspects, most of the results indicate relatively small slip at the hypocenter, large regions of slip near northern Sumatra and near the Nicobar Islands, and a gradual tapering of slip northward beneath the Andaman Islands (Ammon *et al.*, 2005; Ishii *et al.*, 2005; Krüger and Ohrnberger, 2005; Tsai *et al.*, 2005). Analysis and inversion of GPS data indicate similar patterns of slip, although the magnitude of estimated slip is greater than the seismic solutions, potentially owing to aseismic afterslip and postseismic deformation (Banerjee *et al.*, 2005, 2007; Vigny *et al.*, 2005; Subarya *et al.*, 2006). Banerjee *et al.* (2005) show how the radial component of the moment tensor ($M_{rr}$), one of the principal components that governs tsunami generation (Ward, 1982b), varies relative to the observational period—a threefold increase is estimated from centroid moment tensor (CMT) analysis ($T < 300$ sec) to static GPS analysis. Overall, the total moment of the earthquake as deduced from geodetic studies is approximately 9% greater than the long-period seismic moment (Banerjee *et al.*, 2007). As discussed by Kanamori (1972), Ward (1982a), and in this article, tsunami generation is sensitive to longer source process times than seismic-wave excitation, although there is a limit to how slow deformation can occur and still generate a tsunami.

## Variation in First-Order Source Parameters

Both tsunami forecast and assessment models start with a source location and a measured earthquake magnitude (forecast) or estimated scenario magnitude (assessment). The 2004 Sumatra–Andaman earthquake demonstrated that even once the earthquake occurs, there is considerable uncertainty in the magnitude of very large earthquakes, as it would be used for tsunami forecast modeling. Current magnitude estimates range from $M_w$ 9.0 (initial estimate, Lay *et al.*, 2005) to $M_w$ 9.3 (Stein and Okal, 2005). Much of this uncertainty relates to the complex temporal rupture processes, though some of it also relates to uncertainty in fault dip. Michael and Geller (1984) discuss the difficulty in establishing the focal mechanism for shallow thrust earthquakes and the effect that fault dip has on the estimated scalar moment (see also Honda and Seno, 1989; Kawakatsu and Cadena, 1991; Banerjee *et al.*, 2005; Park *et al.*, 2005). Advances in rapidly estimating moment magnitude for tsunami warning have been made by examining first-arrival *P* waveforms ($M_{wp}$) (Tsuboi *et al.*, 1995; Tsuboi, 1999, 2000) and using the variable-period mantle magnitude ($M_m$) (Weinstein and Okal, 2005).

In addition to structural parameters such as fault geometry, other first-order static source parameters needed for tsunami modeling (average slip, rupture length, etc.) are estimated from scaling relationships (Kanamori and Anderson, 1975; Geller, 1976; Wyss, 1979; Scholz, 1982, 1994; Das, 1988; McGarr and Fletcher, 2003; Romanowicz and Rundle, 1993). There is, however, significant uncertainty in these scaling relationships (Geller, 1976), with less known about subduction-zone earthquakes than on-land (typically strike-slip) earthquakes (e.g., Wells and Coppersmith, 1994). Local tsunami runup varies nearly linearly with slip (Geist and Yoshioka, 1996), whereas variations in rupture length affect runup distribution in the near field (Okal and Synolakis, 2004) and amplitude beaming in the far field (Ben-Menahem and Rosenman, 1972; Ward, 1982a; Okal, 1988, 1991; Titov *et al.*, 1999). Ishii *et al.* (2005) notes that the rupture length of the 2004 Sumatra–Andaman earthquake exceeds that for other $M > 9$ earthquakes, although the rupture width appears to be considerably smaller than $M > 9$ continental subduction zone earthquakes ($M$ 9.5 1960 Chile and $M$ 9.2 1964 Alaska). Kajiura (1981) and Geist (1999) demonstrate how other first-order source parameters such as rupture width and dip affect the tsunami wave field.

## Tsunami Forecast Models

### Scalar, Point-Source Representation

Several studies have indicated that far-field tsunami amplitudes can be estimated from the scalar seismic moment of the earthquake (Comer, 1980; Ward, 1980; Okal, 1988; Pelayo and Wiens, 1992). Empirical and theoretical relationships that link far-field tsunami amplitudes with seismic moment include the attenuating effects of geometric spreading as a function of propagation distance ($R$) (Wu, 1981; Mei, 1989). In particular, Abe (1979, 1995) gives an empirical relationship relating the tsunami height (in meters) ($Ht$) to moment magnitude ($M_w$):

$$\log Ht = M_w - \log R - 5.55 + C, \qquad (1)$$

where $C = 0.0$ for interplate thrust earthquakes and $C = 0.2$ for backarc events and where $R$ is in kilometers measured from the epicenter. Because this regression overpredicts tsunami heights in the near field, a local limiting tsunami height ($Hr$) that is independent of distance is established by Abe (1981, 1995):

$$\log Hr = 0.5\, M_w - 3.30 + C. \qquad (2)$$

Abe (1995) indicates that *Hr* statistically represents the mean local runup and that 2*Hr* approximates the maximum local runup. Abe (1995) provides a detailed statistical comparison for local tsunamis, and Furumoto (1996) provides a test for this relationship at far-field distances.

To determine how these empirical relations fare for the 2004 Sumatra–Andaman earthquake, we use $M_w$ 9.0, which was determined soon after the event using 300- to 500-sec-period surface waves (Lay *et al.*, 2005). At regional distances, the far-field relationship (equation 1) for example, slightly underpredicts with mean observed runup heights in southeast India (Yeh *et al.*, 2005) ($Ht = 2.8$ m; 2.5–5.2 m reported) and is consistent with the mean runup heights in Dawei, Myanmar (Satake *et al.*, 2006b) ($Ht = 2.3$ m; 0.9–2.9 m reported). In contrast, along an azimuth in line with the tsunami beaming pattern, the empirical equation (1) greatly underpredicts the mean recorded tsunami runup in Sri Lanka (Liu *et al.*, 2005; Goff *et al.*, 2006) ($Ht = 1.7$ m; 2.5–7.0 m reported). Locally, the mean ($Hr = 16$ m) and maximum limiting runup height ($2Hr = 32$ m) is very close to the runup heights observed along the western Aceh Province of Sumatra (30–35 m) (Borrero, 2005; Tsuji *et al.*, 2005; Jaffe *et al.*, 2006).

The close correspondence of predicted and observed maximum local runup heights is consistent with little scatter in observations for $M > 9$ events using other local tsunami magnitude scales (Geist, 2002), though there are few events in the historical catalog to provide a measure of uncertainty. For more frequently occurring tsunamigenic earthquakes in the range $7.0 < M_w < 8.5$, the uncertainty associated with the empirical relationship greatly increases because of greater variability in source depth, rupture width, and water depth above the source—all parameters that relate to earthquakes with rupture widths smaller than the saturation width of subduction zones. The $M_w$ 8.7 March 2005 Sumatra earthquake is shown to be deficient in tsunami generation compared to other earthquakes of similar magnitude and defines a new lower bound in the scatter for empirical local tsunami relationships at this magnitude (Geist *et al.*, 2006). Therefore, while empirical tsunami relationships provide important mean and maximum tsunami height estimates based only on point-source characterization of the earthquake (magnitude, epicenter), there is considerable uncertainty in these estimates. These statistics also do not yield any information on the site-specific distribution of runup heights that can be ascertained from real-time, finite-source modeling described in the next section.

## Subfault Dislocation Models, Real-Time Tsunami Measurements

The next level of source parameterization for tsunami forecasts are subfault dislocation models. These models specify uniform slip over one-to-several subfaults for calculating the coseismic vertical displacement field. This, in turn, specifies the initial conditions for the tsunami propagation calculations, such as for the forecasting system in the Pacific Ocean (Titov *et al.*, 1999, 2005a). The objective of the forecasting system is to provide site-specific and event-specific forecasts of tsunami wave amplitudes and travel times in real time.

This forecasting system consists of a precomputed propagation database and real-time assimilation of water-level data, primarily from Deep-ocean Assessment and Reporting of Tsunamis (DART) stations. The propagation database consists of basinwide wave-field calculations (amplitude as a function of location and propagation time) from individual subfaults, or unit sources, measuring 50 km wide and 100 km long. Each major subduction zone interplate thrust at seismogenic depths is discretized into unit sources. Fault geometry is estimated from observed seismicity and geophysical studies. Coseismic vertical displacement from the unit sources is used as initial conditions for the Method of Splitting Tsunami (MOST) propagation model (Titov and Synolakis, 1997, 1998). The MOST model is based on a finite-difference numerical approximation to the nonlinear, shallow-water wave equations. For the far-field applications, the equations are transformed into spherical coordinates and the effects of the Coriolis force are added (Titov and González, 1997). Because the equations for both the vertical displacement calculations and offshore tsunami amplitude calculations are dominated by linear terms, variable amounts of uniform slip can be assigned to each unit source, and unit sources can be linearly combined to determine the tsunami wave field for any earthquake of arbitrary magnitude and subfault discretized slip distribution. Sea level observations from the DART data are used to invert the tsunami wave field to determine the slip distribution for any given tsunamigenic earthquake.

In practice, this forecasting system proceeds in four stages once an earthquake of a given magnitude and location occurs: (1) An initial tsunami wave field is determined using the nonlinear MOST model from a number of unit sources with uniform slip, both of which are scaled relative to the earthquake magnitude. (2) The initial source parameterization is refined based on the inversion results from the DART data. (3) Propagation calculations are recomputed based on the refined source. (4) For specific sites (e.g., Hilo, Hawai'i), inundation calculations are performed using a small-scale, finite-difference grid and where the nonlinear propagation terms become increasingly important. The latter step is a boundary-value problem in which the offshore linear wave-field is used as a boundary condition for the small-scale inundation calculations (Titov and Synolakis, 1998). Titov *et al.* (1999, 2001) present the results of sensitivity analyses indicating that other source parameters such as rake angle have a secondary influence on far-field tsunami amplitudes, in comparison to slip and rupture length.

To determine how tsunami estimates from a subfault parameterization for the 2004 Sumatra–Andaman earthquake compare to observations, Titov *et al.* (2005b) divides the 1300-km-long rupture zone into four subfaults (Fig. 2a).

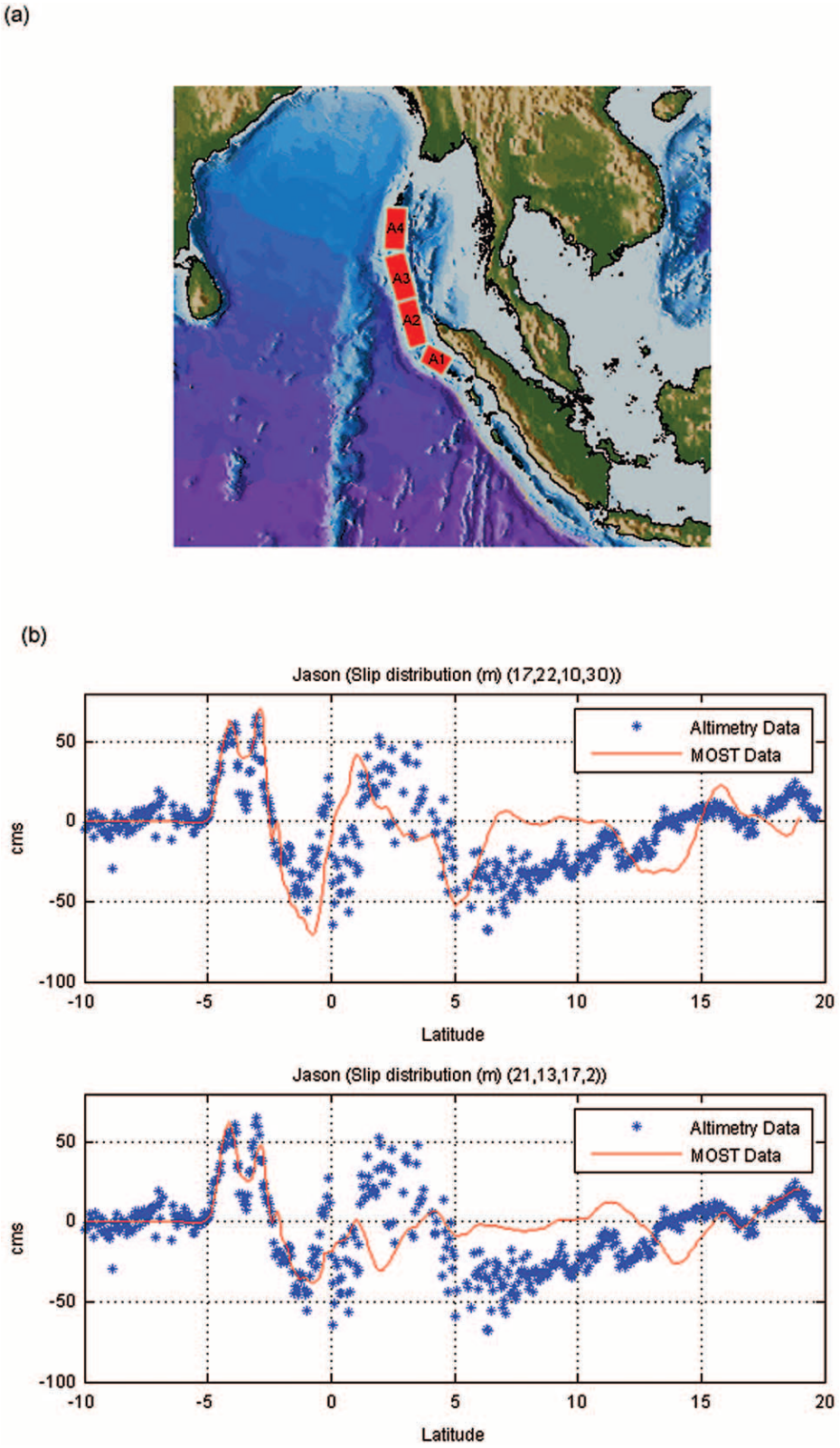


Figure 2. (a) Subfault discretization of the 2004 Sumatra–Andaman earthquake. (b) Comparison of computed tsunami heights (red line) along Jason-1 trackline (Fig. 1) in comparison to the altimetry measurements (*). *Top*: Rms best fit to all data; *Bottom*: Rms best fit to direct arrivals (see Fig. 3). Values of slip for each subfault (south to north) indicated above figure.

This source characterization is similar to that used for analyzing static offsets in the GPS data (Banerjee *et al.*, 2005). Slip for each subfault is constrained by the Jason-1 satellite altimetry measurements that record a transect of the tsunami wave field approximately 2 hr after the earthquake (Gower, 2005). The phases recorded on the satellite altimetry record include both direct arrivals south of the equator as well as reflections from coastlines and submarine topographic features such as the Ninetyeast Ridge (Fig. 1). An interpretation of the direct arrival phases is shown in Figure 3. At greater distances, Hanson and Bowman (2005) also detect reflections from other bathymetric features such as the Mascarene Plateau between the Seychelles and Mauritius Islands from hydrophone records. Fault slip is constrained from both the rms prediction error of all phases (Fig. 2b, top) resulting in a slip distribution of 17, 22, 10, and 30 m, respectively on each fault segment taken from south to north, or from the direct arrival (Fig. 2b, bottom) with an associated slip distribution of 21, 13, 17, and 2 m on each segment. A map showing the maximum tsunami amplitude in the Indian Ocean over 10 hr of propagation time is shown in Figure 4a. Titov *et al.* (2005b) note that this level of source parameterization adequately estimates regional and far-field tsunami travel times and amplitudes.

In addition, as a test of the inundation calculations (stage 4 of the forecast model described previously), the subfault source model with the slip distribution shown in Figure 2b (top) is used to hindcast inundation at Banda Aceh. The fine-scale bathymetric/topographic elevation database for this calculation was compiled from digitized bathymetric charts, shuttle radar mission elevation data, and other sources. Using the same source description that provides a fit to the Jason-1 deep-ocean tsunami measurements, the extent of inundation is well predicted in comparison to satellite imagery of the inundated region (Fig. 4b). Flow depths and runup heights are also reasonably estimated in comparison to results from the international tsunami survey team (Borrero, 2005; Tsuji *et al.*, 2005; Jaffe *et al.*, 2006). This comparison indicates that a forecasting system based on subfault parameterization can adequately forecast tsunami amplitudes and inundation, given initial information on first-order earthquake parameters and deep-ocean tsunami measurements. It should be emphasized that both sources of information are necessary for this system to perform well.

## Tsunami Assessment Models

For assessing future tsunami hazards, *a priori* earthquake information discussed in the previous section for forecast models is not available. From a tsunami assessment

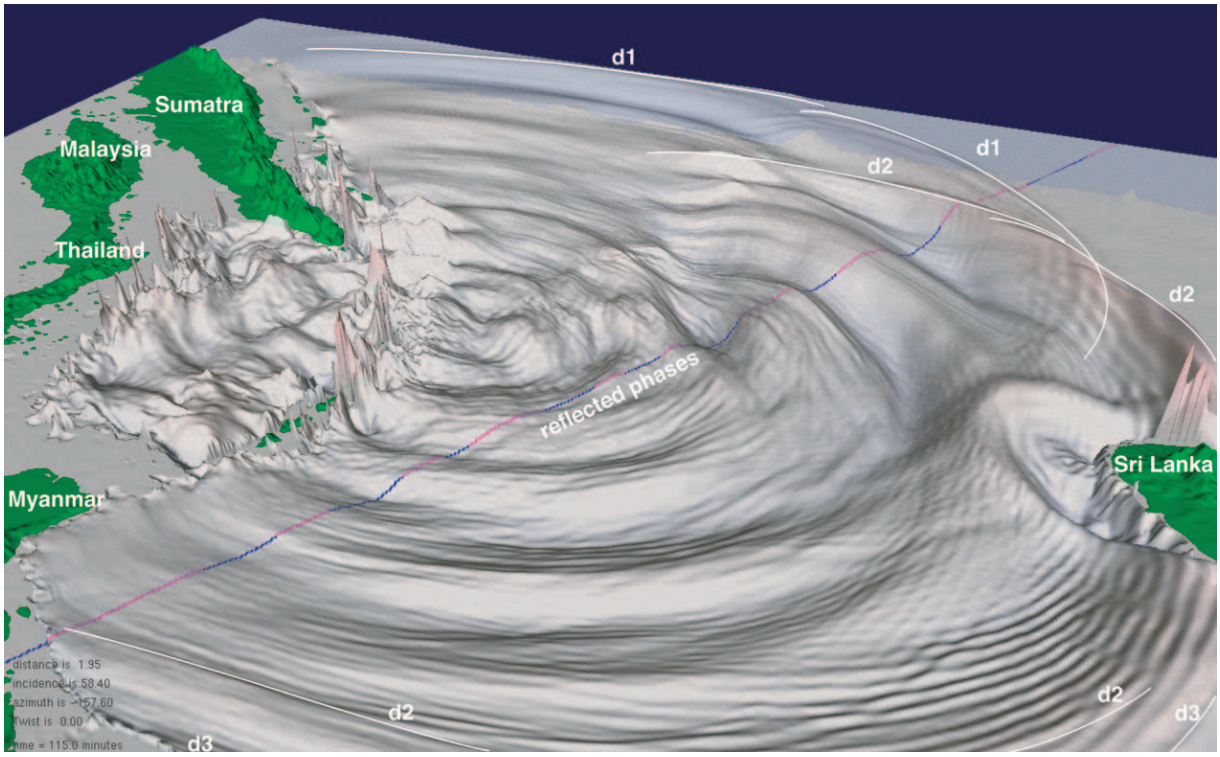


Figure 3. Perspective view of synthetic tsunami wave field 115 min after generation, using the $M_w$ 9.15 source model from Chlieh *et al.* (2007). Line represents Jason-1 satellite altimetry trackline (blue-modeled negative phase; pink-modeled positive phase). Interpretation of direct-arrival phases indicated by white lines: d-1, d-2, and d-3 correspond to regions of high slip in the source model (1, southern slip patch; 2, slip patch near Nicobar Islands; 3, slip patch near Andaman Islands).

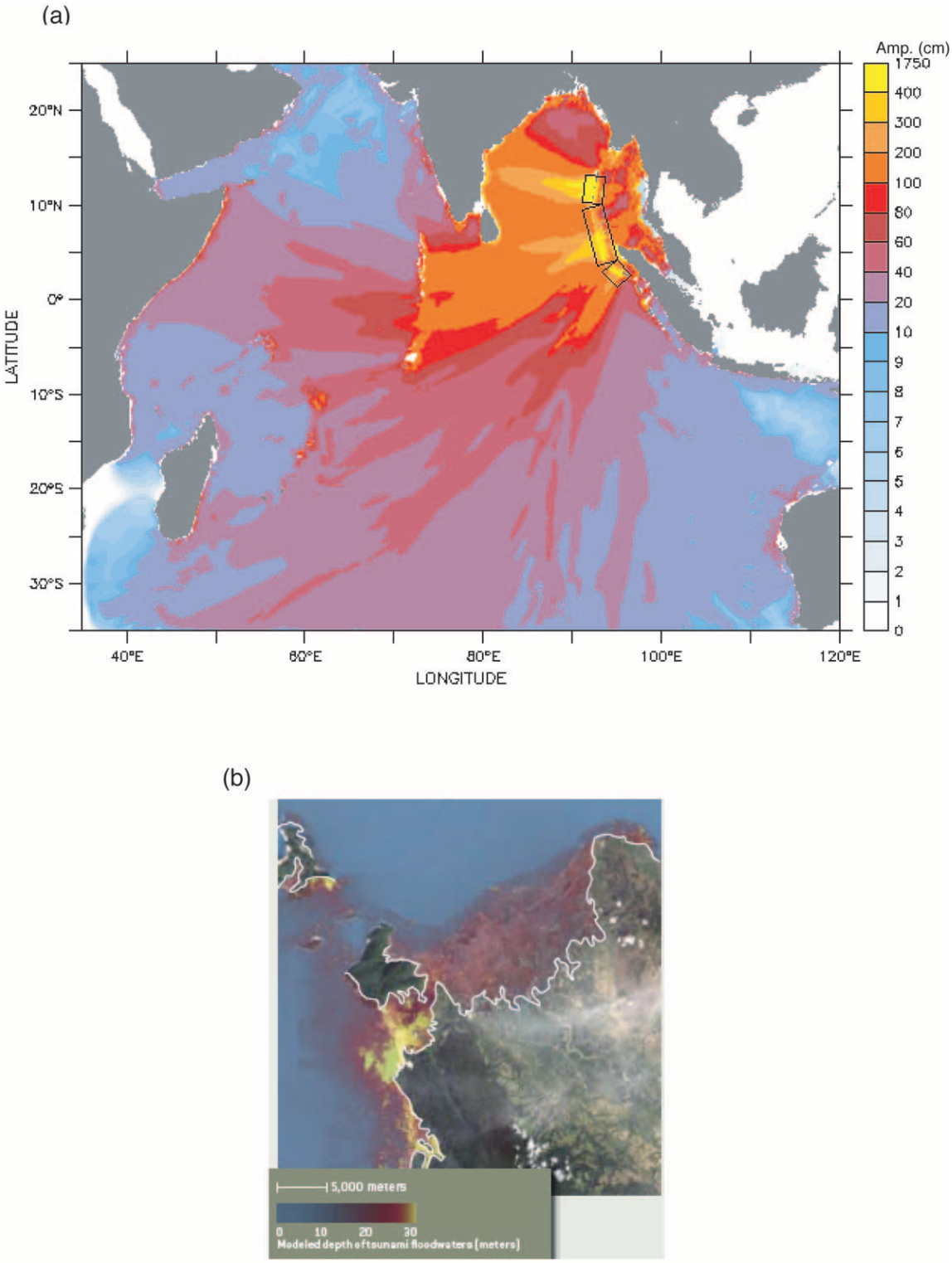


Figure 4. (a) Maximum tsunami amplitude over 10 hr of propagation time, using the subfault geometry shown in Figure 2a and slip constrained, by Jason-1 satellite altimetry (Fig. 2b, top). Wave height is in centimeters. See Titov *et al.* (2005b) for details. (b) Inundation hindcast at Banda Aceh from this source model. White line represents landward inundation limit determined from satellite imagery.

standpoint, we estimate the range of tsunami amplitudes associated with uncertainty in primarily slip and rupture length for a $M_w$ 9.0–9.3 earthquake along the Sumatra–Andaman subduction zone. From a seismic moment–based perspective, uncertainty in shear modulus and slip-length scaling in general leads to uncertainty in $\bar{u}$ (average slip). Because of the lack of data defining scaling relationships for earthquakes of this size, we draw upon several studies of the 2004 Sumatra–Andaman earthquake in addition to studies of $M \geq 9$ earthquakes prior to 2004. In the next section we examine how other source parameters in addition to slip and rupture length affect tsunami estimates.

## Methodology

The effect of coseismic slip is examined both in terms of scaling of average slip with respect to magnitude and the variability of spatially heterogeneous slip patterns. Heterogeneous slip distribution patterns are evident from seismic inversions of major earthquakes, as well as theoretical studies examining the dynamics of earthquake rupture. The combination of effects from physical heterogeneities with nonlinear dynamics of rupture results in mix of characteristic and noncharacteristic modes of slip distributions noted in both theoretical studies (Ben-Zion and Rice, 1995, 1997; Zheng and Rice, 1998; Nielsen and Carlson, 2000; Perfettini *et al.*, 2001; Shaw, 2004) and observational studies specific to subduction zone earthquakes (Thatcher, 1990; Mendoza, 1993; Boyd *et al.*, 1995; Schwartz, 1999; Mazzotti *et al.*, 2000; Hirata *et al.*, 2004; Satake *et al.*, 2006a). Recent studies have also indicated that spatial heterogeneity at scales smaller than typically resolved in seismic and geodetic inversions ($\leq$1 km) (cf., Perfettini *et al.*, 2001) can have a significant effect on near-field static displacement (Honda and Yomogida, 2003; Fu and Sun, 2004). Small-scale spatial heterogeneity in slip translates to variations in local tsunami runup, though the effects are diminished with increasing propagation distance and source depth (Titov *et al.*, 2001; Geist, 2002).

The stochastic source model developed by Andrews (1980) and refined by Herrero and Bernard (1994) is used to determine the variations in offshore tsunami waveforms and peak tsunami amplitudes, in a manner as described by Geist (2002, 2005). Tsunami generation models used for tsunami assessments such as presented here have been modified from models previously used for strong ground motion studies (Herrero and Bernard, 1994; Berge *et al.*, 1998; Somerville *et al.*, 1999; Hisada, 2000, 2001; Honda and Yomogida, 2003). At low wavenumbers, stochastic slip distributions are scaled relative to average slip or static stress drop. Tsunami generation is less affected by the high wavenumber characteristics of slip distribution in comparison to strong ground motion.

For each case examined, one hundred slip distributions ($u(x,y)$) are computed on a 7.5-km fault grid extending along the Sunda trench to a down-dip width of 150 km. Each of the slip distributions conform to a $k^{-2}$ radial-wavenumber spectrum for $k > k_c$ where $k_c$ scales with the characteristic rupture dimension (Herrero and Bernard, 1994; Tsai, 1997; Somerville *et al.*, 1999; Hisada, 2000, 2001; Mai and Beroza, 2002). For the more general case of a $k^{-\alpha}$ spectrum, Zeng *et al.* (2005) note that scaling of $\bar{u}$ with rupture length ($L$) is physically related to the degree of slip heterogeneity ($\alpha$) and indicate that linear scaling between $\bar{u}$ and $L$ occurs only for relatively smooth slip distributions.

For each slip distribution, the coseismic displacement field is calculated based on Okada's (1985) point-source expressions for an elastic half-space. While these expressions are adequate in the near field, displacement models based on a layered spherical geometry are more appropriate at regional and far-field distances (Pollitz, 1996; Banerjee *et al.*, 2007). Because horizontal displacements are large for this event and there are steep bathymetric gradients in places near the source region (Fig. 1), their combined effect is included in the initial conditions to the tsunami propagation model as described by Tanioka and Satake (1996). To accommodate the large number of cases that are run (approximately 1000), the computationally efficient finite-difference approximation to the linear-long wave equations is implemented on a 2 arc-minute bathymetric grid (ETOPO2), using a timestep of 10 sec to satisfy the Courant–Friedrichs–Lewy stability criterion (Satake, 2002). Reflection boundary conditions are imposed at the 50 m isobath, which approximately represents the limit of accuracy of ETOPO2 bathymetry and the validity of the linearized form of the shallow-water wave equations. This type of modeling is often termed "threshold modeling." Radiant boundary conditions are imposed on the open-ocean boundaries (Reid and Bodine, 1968). For each run, the maximum tsunami amplitude during propagation is tracked at the 50 m isobath, termed "peak nearshore tsunami amplitude."

## Results

Tsunami amplitudes at local and regional distances are calculated for four cases, representing two different end members for both average slip and rupture length. To establish the higher end member of average slip, we use high average slip values that are needed to explain the direct arrival south of the equator on the Jason-1 record (Fig. 2b, 3) as indicated by the inversion of Hirata *et al.* (2006) (13.4 m), the subfault forecast model presented here (13.2–19.8 m), and from the stochastic source model (16 m). In addition, relatively high values of uniform slip (19–21 m) are used to explain tsunami observations in Japan from the 1700 Cascadia earthquake of comparable magnitude ($M \sim 9$) (Satake *et al.*, 2003). For the lower estimate, the average slip from tsunami inversions using both satellite altimetry and tide gauge data is 5.5–8.7 m (Fujii and Satake, 2007) and 9.2 m (Tanioka *et al.*, 2006). In addition, the average slip for the $M$ 9.2 1964 Alaska earthquake is 8.6 m (Johnson *et al.*, 1996). From this, we consider end members of 9 m and 16 m

for average slip. For rupture length, we use 900 km as a lower bound, from both the inverse tsunami travel time (Kowalik *et al.*, 2005; Neetu *et al.*, 2005) and the primary region of uplift (Model III, Ammon *et al.*, 2005) for the 2004 Sumatra–Andaman earthquake. The rupture length for 1964 Alaska earthquake was approximately 700 km, though the rupture width was much greater (200–300 km) than the 2004 Sumatra–Andaman earthquake (Johnson *et al.*, 1996). For the upper bound, we use a rupture length of 1600 km, as indicated by the emergence and subsidence of coral reefs following the 2004 event (Meltzner *et al.*, 2006). Taken together, these four cases span the magnitude range $9.0 \leq M \leq 9.3$, assuming a shear modulus of 30 GPa.

For the $\bar{u} = 9$ m, $L = 1600$ km case, mean and extrema peak nearshore tsunami amplitude are displayed in Figure 5 as a function of latitude for four different coastline segments. In general, the variation in nearshore tsunami amplitude decreases with distance from the source, consistent with the sensitivity analysis of Titov *et al.* (1999, 2001), and is most pronounced for local tsunamis near the source region. Also shown in Figure 5 are synthetic marigrams (amplitude as a function of time) at representative offshore locations. Similar to the nearshore tsunami amplitude plots, the marigrams show the mean and extrema amplitudes and indicate expected variation in waveforms. Significant phase shifts among time series in the ensemble are indicated where the extrema values are not parallel with the mean value marigram (e.g., Phuket). The frequency content of the marigrams is dependent on the propagation path (obliquity of incidence) and the nearshore response, in particular, the excitation of trapped (edge waves) and reflected modes (Fujima *et al.*, 1995; Rabinovich, 1997; Liu *et al.*, 1998; Koshimura *et al.*, 1999).

Results from using a shorter rupture length and higher slip (Fig. 6), shows significant variations in comparison to the previous case (Fig. 5). In both cases, $M_w$ 9.14 $\pm$ 0.02, such that the differences are not attributable to changes in overall magnitude. Increasing the slip value results in a significant increase in tsunami amplitudes, particularly at sites in line with the beaming pattern emanating from the southern part of the fault where the 900 km and 1600-km-long faults overlap. Decreasing the rupture length partially compensates for the increase in runup values in the northern part of the study region, particularly offshore Myanmar.

We also compare results from varying average slip and rupture length to observed runup from the international tsunami survey teams. This can only be a qualitative comparison for several reasons. Accurate determination of tsunami runup from offshore amplitude values is greatly dependent on nearshore propagation effects and as such, detailed inundation modeling depends on the availability and accuracy of fine-scale (~30–100 m horizontal resolution) nearshore bathymetry and coastal topography. Data at this resolution does not currently exist for most of the coastlines affected by the Indian Ocean tsunami. Small-scale variation in nearshore topography can result in extreme variations in runup as shown by Titov and Synolakis (1997) for the 1993 Hokkaido tsunami. In addition, for large tsunamis such as the 2004 Indian Ocean tsunami, turbulent dissipation in the nearshore region and during propagation across shallow continental shelves may have a significant effect on runup. As an approximation, we use an amplification parameter that translates offshore tsunami amplitudes to runup that has been previously be applied to threshold models (Shuto, 1991; Satake, 1995). The value of the amplification parameter is typically 2–3 for coarse grid calculations, although it can locally be greater, depending on nearshore bathymetry (Satake, 1995).

The results of three cases ($\bar{u} = 9$ m, $L = 1600$ km; $\bar{u} = 16$ m, $L = 900$ km; and $\bar{u} = 16$ m, $L = 1600$ km) are compared to the runup observations for 11 sites, using an amplification parameter of 2 (Fig. 7). Runup measurements in the Nicobar and Andaman Islands represent only single-site measurements (Jain *et al.*, 2005). For comparison, we also show the mean runup estimate using scalar, point-source forecast (Abe, 1995) and for 9 m and 16 m of uniform slip ($L = 1600$ km). The point-source forecast is based on the distance from the epicenter, except near the source region where the local, limiting height equation (2) is used (Abe, 1995).

In general, the tsunami from using the smaller average slip (9 m) and longer fault (1600 km) is consistent with runup values in most regions except western Aceh where it does not predict the extreme runup values and Myanmar where it overpredicts runup. The 16-m average slip model matches the runup in western Aceh well, although it tends to overpredict runup everywhere else. This is not unexpected, since large values of maximum slip (20–30 m) have been resolved in the southern part of the rupture zone from seismic, geodetic, and tsunami inversions and since the 16-m higher-end average slip estimate is based in part from the direct arrival emanating from the southern slip patch as observed on the Jason-1 altimetry profile (2°–5° S, Figs. 2 and 3). The overestimation of runup in Myanmar and Thailand can be partially compensated by using a smaller rupture length (Satake *et al.*, 2006b), though the $\bar{u} = 16$ m, $L = 900$ km still overpredicts runup in these locations. It should be also noted that the broad shelf and complicated bathymetry offshore Thailand and Myanmar (Mergui Terrance, Fig. 1) will likely have a measurable effect on the results. In such regions, tsunami attenuation may occur through dispersion (Shibata, 1983) and turbulent dissipation after breaking (Synolakis and Skjelbreia, 1993). Because we do not account for these effects in the linear assessment model used here, tsunami runup may be overestimated in this region. For the uniform displacement models, using a slip value of 9 m tends to underpredict the local tsunami amplitudes, whereas a value of 16 m tends to overpredict the regional tsunami amplitudes (Fig. 7). As mentioned previously, the scalar, point-source estimate generally does well, except for sites on the main beam of tsunami energy.

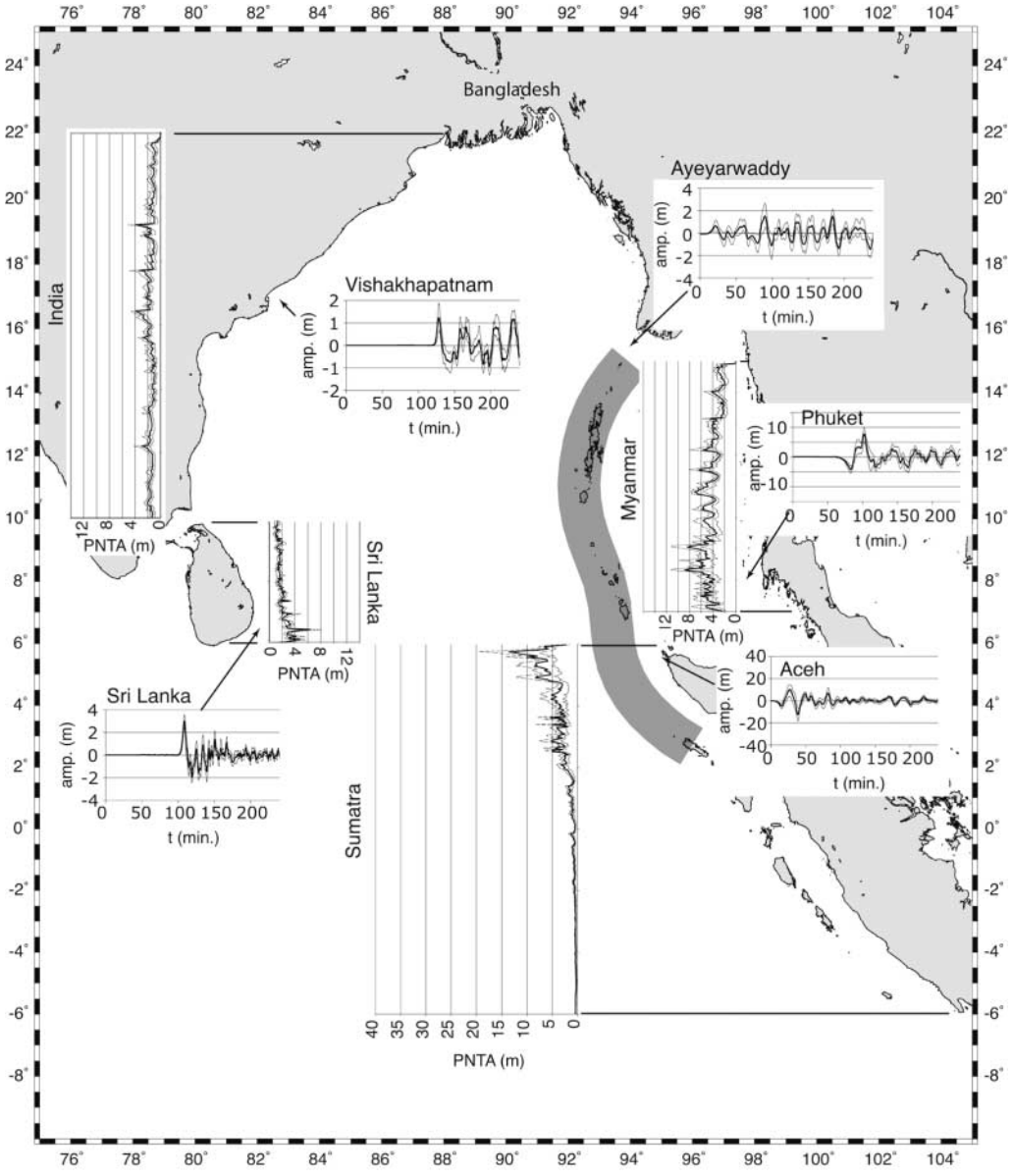


Figure 5. Peak nearshore tsunami amplitude and synthetic nearshore marigrams in the Bay of Bengal for the $\bar{u} = 9$ m, $L = 1600$ km case ($M_w$ 9.14). Variations in nearshore tsunami amplitude are shown as a function of latitude for four coastlines (average, heavy line; extrema, light lines). Variations in marigrams (average, heavy line; extrema, light lines) for five representative location also shown.

## Effects of Secondary Source Parameters on Forecast and Assessment Models

### Shallow Rupture Properties

As with slip distribution, it is difficult to know various aspects of shallow rupture, such as surface rupture or splay faulting, prior to the event (assessment models) or even shortly after the occurrence of an earthquake (forecast models). For ideal crack models, the circumstance of surface rupture results in a fundamentally different slip distribution in the dip direction, because of the traction-free boundary condition at the surface (Dmowska and Kostrov, 1973; Rudnicki and Wu, 1995). For these crack models, the maximum and average slip doubles in amplitude with the circumstance of surface rupture, although there is not a corresponding difference in the vertical displacement field (Geist and Dmowska, 1999). The stochastic source used previously is developed with a smooth taper in slip toward both the up-dip and down-dip edges of the rupture zone (as well as near the rupture ends along strike). To test the effect that surface rupture has on the regional tsunami wave field, we modify the standard stochastic source model to remove the slip taper at the up-dip edge. This is performed by computing a stochastic slip distribution for a fault that is twice as wide, and

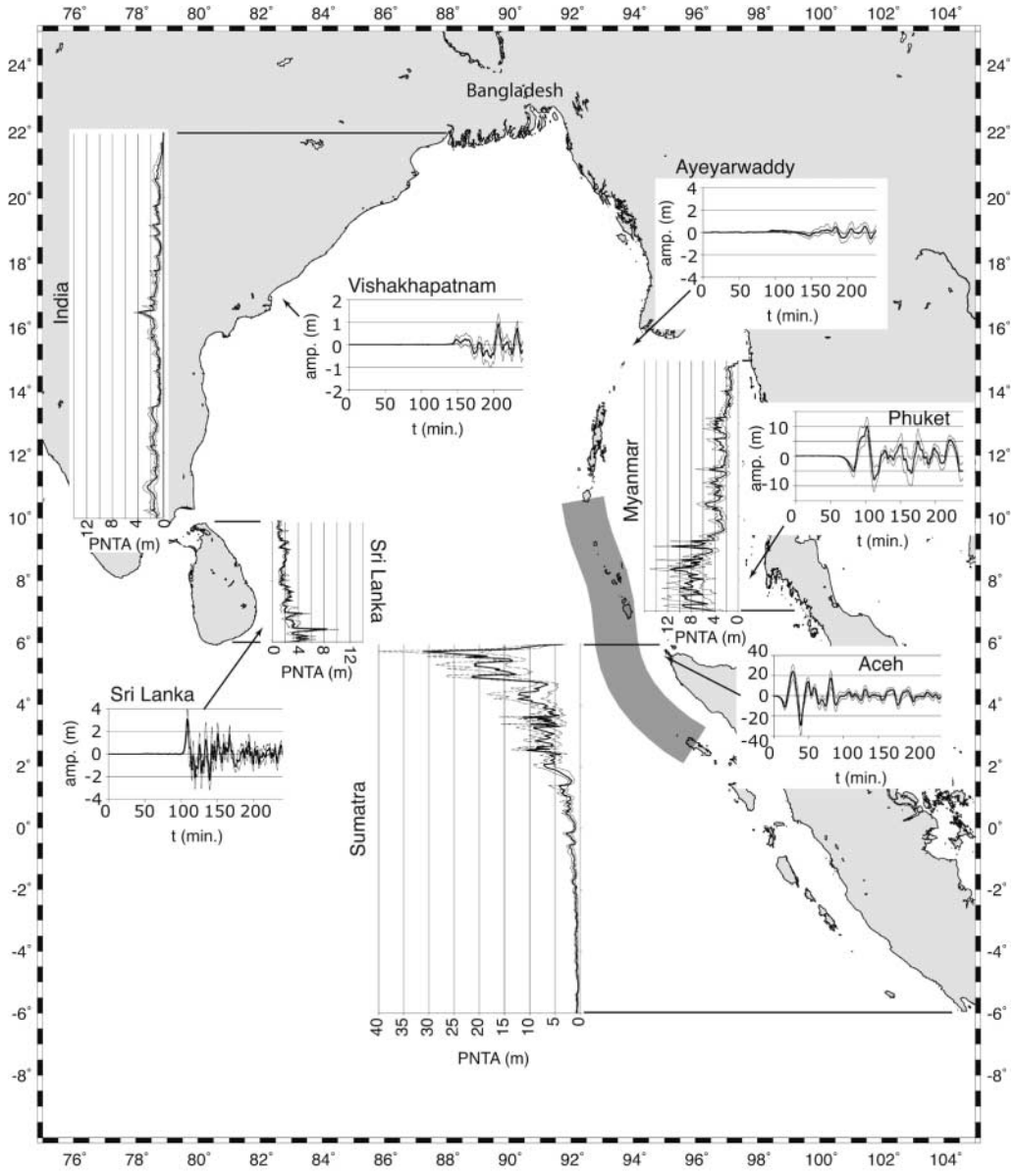


Figure 6. Same as Figure 5 for the $\bar{u} = 16$ m, $L = 900$ km case ($M_w$ 9.14).

using only the down-dip half of the slip distribution as input to the coseismic displacement and tsunami computations. This also simulates the fundamental shift from a half-ellipsoidal to quarter-ellipsoidal shape for the down-dip slip distribution predicted for a surface-rupturing earthquake (Rudnicki and Wu, 1995). Results shown in Figure 8 for two different slip distributions indicate that the surface-rupture model produces slightly higher tsunami amplitudes in the source region in comparison to the imbedded-rupture model. There is also a broadening of the zone of uplift commensurate with the shift to the quarter-ellipsoidal shape of the down-dip slip distribution. This pushes the hingeline of coseismic vertical displacement farther to the east from its position for the imbedded rupture. The position of the hingeline for the December 2004 earthquake determined from satellite imagery of coral microatolls (Meltzner *et al.*, 2006) is most consistent with that for the imbedded rupture.

Local and regional modeling of tsunamis from surface-rupturing events (Fig. 9) yield interesting results in comparison to that for standard imbedded ruptures (Fig. 5). For the eastward propagating tsunamis (nominally, the leading-depression wave), tsunami amplitudes are higher for the simulated surface-rupturing events in comparison to imbedded ruptures. In addition, the amplitude variation caused by different slip distribution patterns is greater. In contrast, for westward-propagating tsunamis (nominally, the leading-elevation wave), tsunami amplitudes are slightly lower for surface-rupturing events. One explanation for this is that, whereas the overall vertical displacement from a surface rupture is slightly greater than that for an imbedded rupture, the

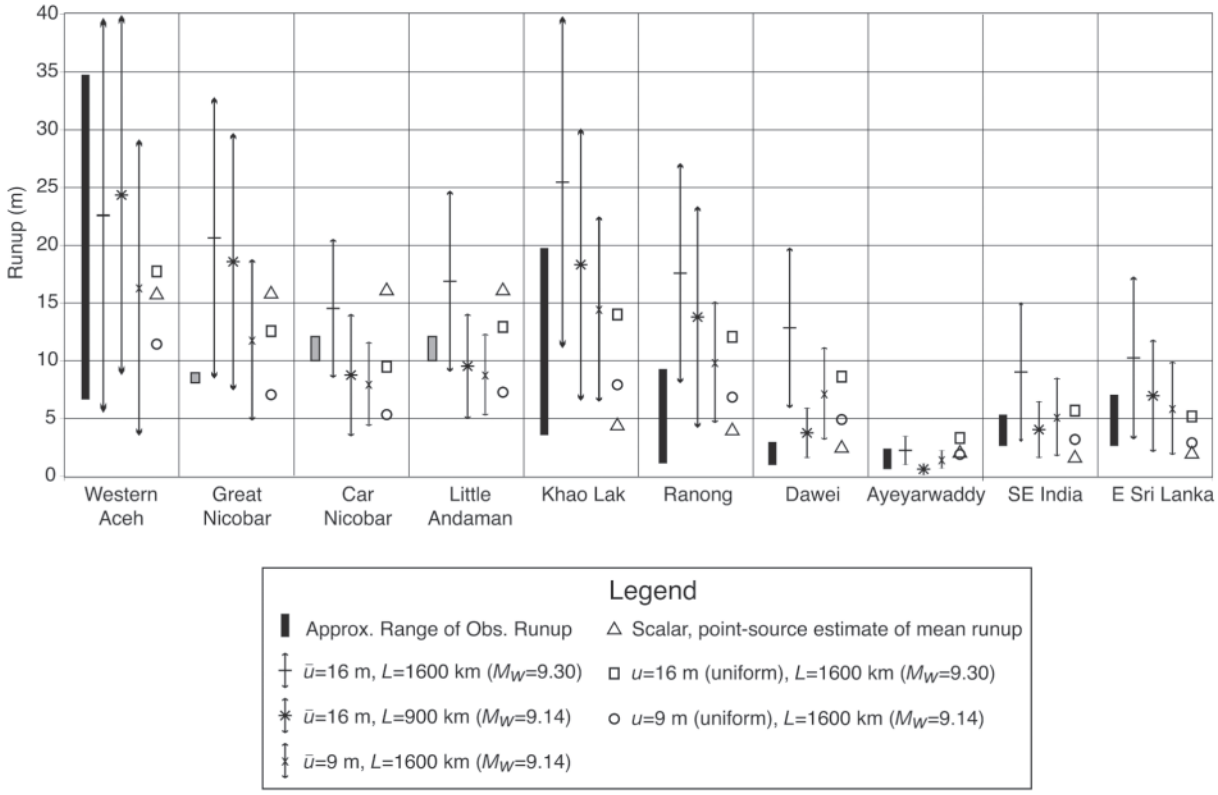


Figure 7. Comparison of tsunami runup observations (black bars, gray for single location observations) with estimates from three sets of end-member source parameters using the stochastic source model. Modeled runup is approximated by applying an amplification factor of 2 to the peak nearshore tsunami amplitudes. Range for each model is caused by variation in slip distribution patterns and propagation paths from subevents. Also shown for comparison are mean runup estimates from Abe's (1995) expression (triangle) and mean runup from uniform slip models: 9 m (circle) and 16 m (square). Approximate latitude range and reference for runup surveys are as follows: western Aceh, 4.6°–5.7° N (Borrero, 2005; Tsuji *et al.*, 2005; Jaffe *et al.*, 2006); Great Nicobar, Car Nicobar, and Little Andaman (Jain *et al.*, 2005); Khao Lak 8.3°–9.2° N (Tsuji *et al.*, 2006); Ranong, 9.2°–10.0° N, Dawei, 13.6°–14.1° N, and Ayeyarwaddy 15.7°–15.8° (Satake *et al.*, 2006b); Southeast India 10.4°–13.4° N (Yeh *et al.*, 2005); East Sri Lanka, 6.7°–8.8° N (Liu *et al.*, 2005; Goff *et al.*, 2006). (See Fig. 1 for locations.)

steep leading wavefront associated with the westbound wave may collapse during propagation, owing to the effects of frequency dispersion. Whether the reduced peak nearshore tsunami amplitude values associated with the westward propagating waves can be ascribed solely to the characteristics of the leading wave, however, is unclear.

Another important aspect of shallow rupture is how seismic moment is distributed at shallow depths in subduction zones. Through the derivation of tsunami eigenfunctions, Okal (1988) indicates that if 10% of the moment release occurs in a low-rigidity sediment layer, tsunami excitation can increase by an order of magnitude. In a series of studies, the systematic increase in rupture duration for shallow subduction zone earthquakes of decreasing focal depth is linked to depth-dependent material properties and lateral heterogeneities along the plate interface (Tanioka *et al.*, 1997; Bilek and Lay, 1999, 2000; Polet and Kanamori, 2000; Bilek and Lay, 2002; Bilek *et al.*, 2003). Although it is unclear whether the increase in rupture duration is related to changes in stress drop or shear modulus (Bilek and Lay, 1999), the latter would result in significantly different tsunami generation from a moment-based characterization of the earthquake (Geist and Bilek, 2001). Because in this case, we are using slip-based earthquake models, the effects of material heterogeneity do not result in large differences in tsunami generation as they would for moment-based models. Examination of earthquakes from 1992 to 2004 in the Sumatra–Andaman source region by Bilek (2007), however, indicate significant along-strike variation in source durations, suggesting accompanying along-strike variations in frictional conditions.

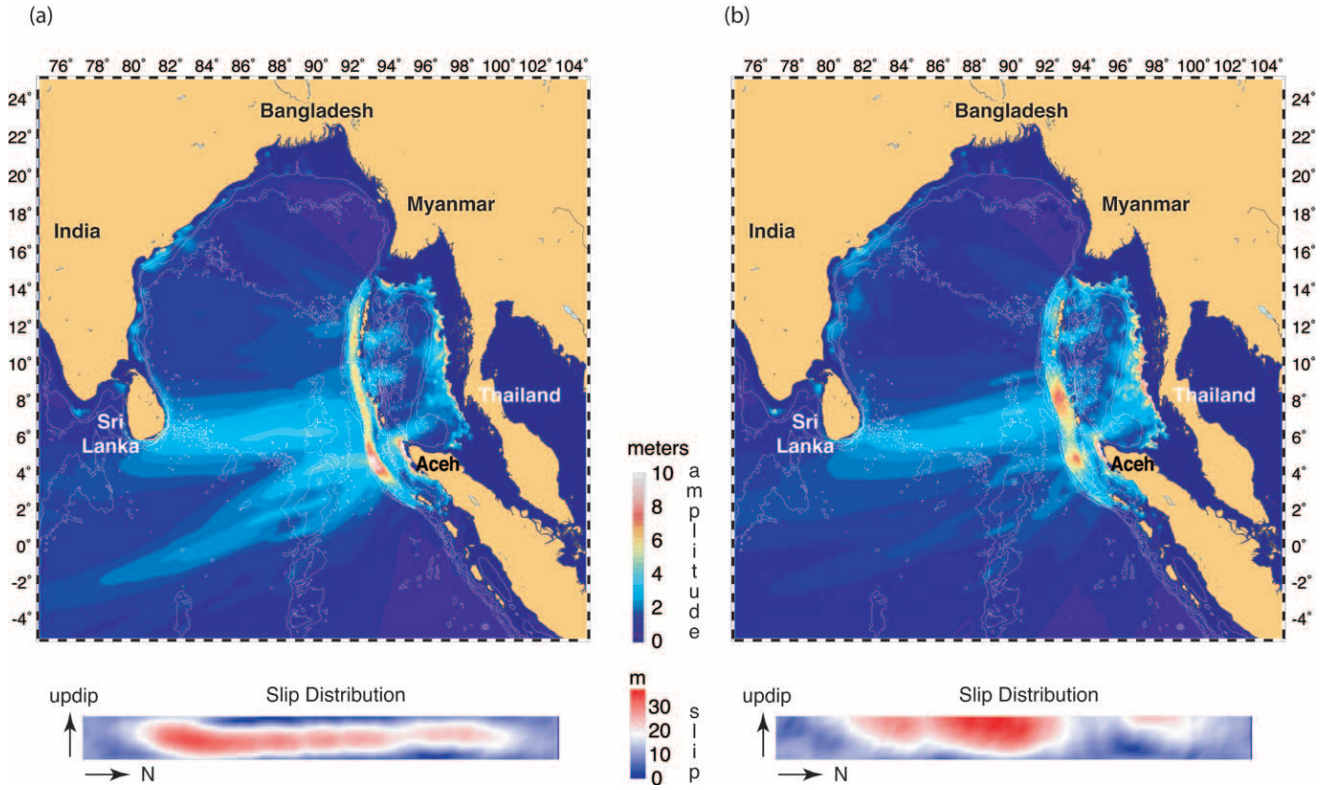


Figure 8. Maximum tsunami amplitude over 4 hr of propagation time for two different slip distributions (bottom). (a) Standard stochastic source model with standard imbedded rupture; (b) modified stochastic source model for a surface rupture (no slip taper near the trench).

### Variations in Rake

For oblique subduction zones such as the Sumatra–Andaman segment, variations in rake angle are expected. Without prior information on the December 2004 earthquake, general models for rake distribution based on tectonic analysis such as McCaffrey (1992) can be used. In this study, he indicates that the slip vector will approximately be aligned with the direction of relative plate motion up to a critical angle $\Psi_{max}$ measured with respect to the trench normal. For Sumatra, McCaffrey (1992) indicates that $\Psi_{max} =$ 15°–25°. We compare the tsunami wave field for the assumption of pure thrust for the entire rupture length with a case where the rake is assumed to vary linearly south to north from 90° to 115°. The latter case represents a greater variation than what was used by Banerjee *et al.* (2005) for the three subfault characterization, but less than the maximum variation used by Banerjee *et al.* (2007) in the subdiscretization of the Andaman segment. Results indicate the variations in rake only slightly affect the maximum tsunami amplitudes (<1 m difference) for the range tested, consistent with the results of Titov *et al.* (1999, 2001).

### Temporal Earthquake Rupture Processes

Because tsunami phase speeds are considerably slower than earthquake rupture velocities, tsunami generation is often assumed to occur instantaneously. For great earthquakes with unilateral rupture propagation, however, the rupture duration will be of sufficient magnitude to affect tsunami travel times. In addition, there is weak directivity of tsunami amplitudes in the direction of rupture propagation for time-dependent tsunami generation models (Geist, 1999). Again, the direction of rupture propagation cannot be reliably predicted ahead of time for most subduction zone earthquakes, although one may be able to determine rupture propagation direction from seismic analysis, such as the second-degree seismic moments (McGuire *et al.*, 2001), soon after the event. An illustration of the effect that rupture direction has on tsunami amplitudes is shown in Figure 10, where south-to-north unilateral rupture (Fig. 10a) is compared with north-to-south unilateral rupture (Fig. 10b). For each case, an identical slip distribution and rupture velocity (2.5 km/sec) are used. In addition to the slight increase in near-field tsunami amplitudes in the direction of rupture propagation, there is a noticeable rotation in the regional tsunami beaming pattern. These effects of rupture propagation on the tsunami wave field increase with decreasing rupture velocity (Geist, 1999).

The other temporal effect that has been noted from geodetic studies is potential afterslip along the fault occurring at periods beyond those that are typically observed by analysis of seismic waves. Banerjee *et al.* (2007) estimate a 9%

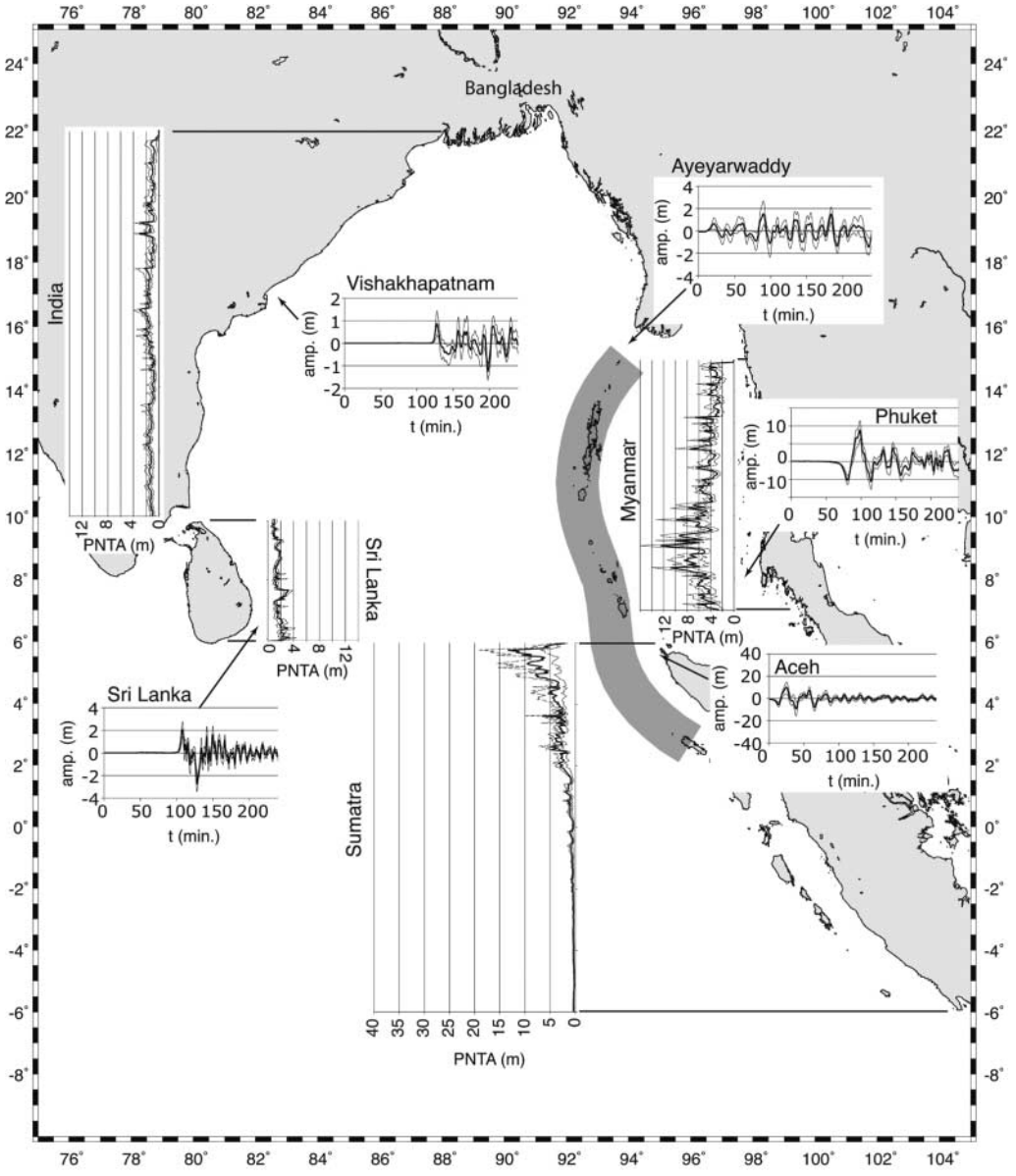


Figure 9. Same as Figure 5 for a 1580-km-long rupture that ruptures to the free surface (trench). Mean slip is identical to the case of Figure 5, such that $M_w$ 9.14.

excess moment release (reckoned to 1 day after the earthquake) for the 2004 Sumatra–Andaman earthquake in comparison to seismic moment estimates. There have been suggestions from studies of previous earthquakes that short-term afterslip may occur at time periods that affect tsunami generation (Kikuchi *et al.*, 1993; Heki and Tamura, 1997; Kato and Ando, 1997; Mazzotti *et al.*, 2000; Miyazaki *et al.*, 2004). For tsunami earthquakes in particular, long source duration is often ascribed to both anomalously low rupture velocities and slow slip rates (Kanamori, 1972; Kikuchi and Kanamori, 1995). The 2004 Sumatra–Andaman earthquake seems to share anomalous slow rupture processes that have been associated with tsunami earthquakes (Seno and Hirata, 2007) and other $M > 9$ earthquakes such as the 1960 Chile earthquake (Cifuentes, 1995; McCaffrey, 1997).

To determine the effect that slow rupture processes have on tsunami generation, we calculate tsunami evolution along a one-dimensional (1D) transect across the southern rupture zone (Fig. 11a) where long duration earthquakes have been observed, both pre and post 2004, possibly representative of slow slip processes (Bilek, 2007). Evolution of slip ($D(t)$) at the point where the transect crosses the fault zone is given by the following expression (Kanamori, 1972):

$$D(t) = D_0\left[1 - \exp\left(\frac{-t}{\tau}\right)\right],$$

where $D_0$ is the static value of slip and $\tau$ is a time constant. (At $t = \tau$ and $t = 2\tau$, about 63% and 86% of total slip is achieved, respectively.) Tsunami waves are modeled using

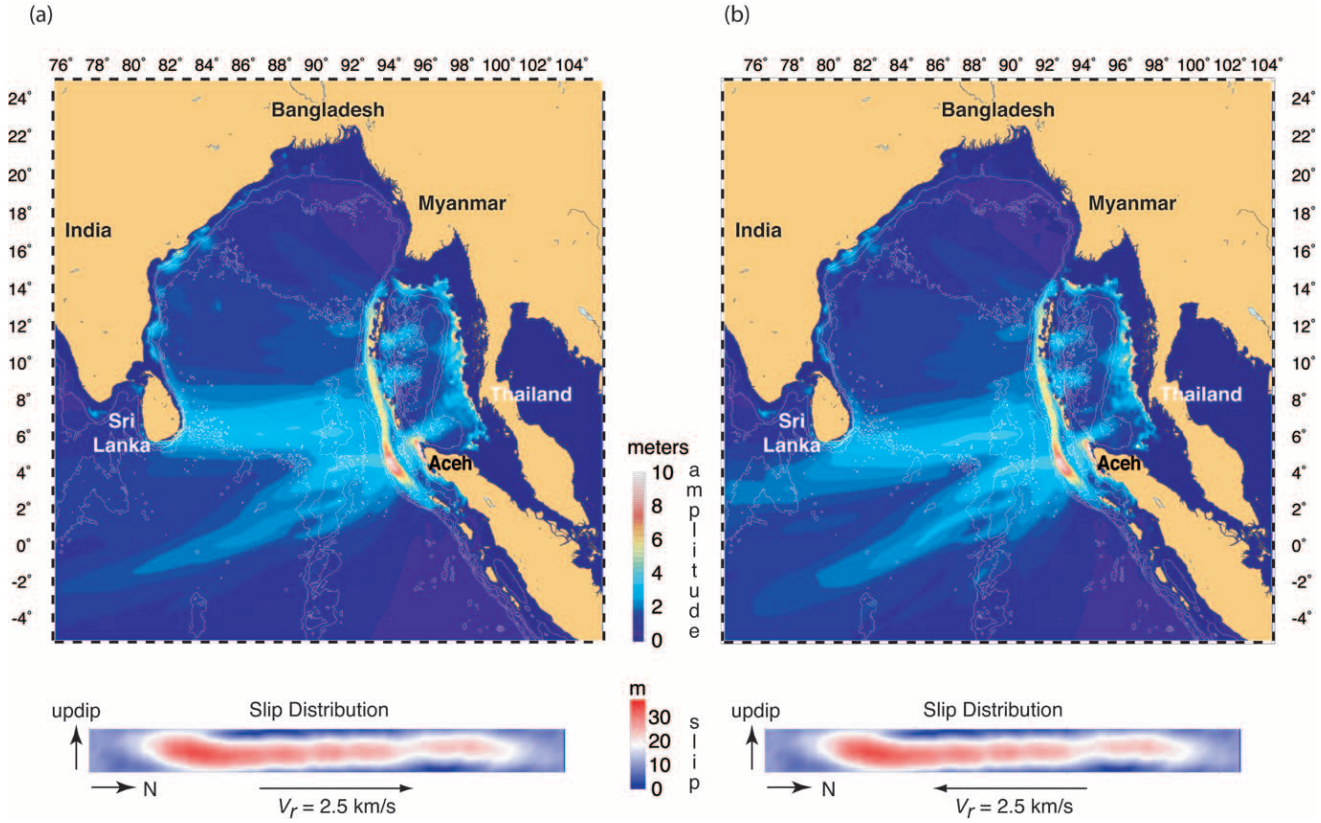


Figure 10. Comparison of rupture direction assumption on maximum tsunami amplitude over 4 hr. (a) South-to-north unilateral rupture; (b) north-to-south unilateral rupture. In both cases, identical slip distribution and rupture velocity (2.5 km/sec are used (bottom).

the nonlinear, dispersive form of the 1D shallow-water wave equations given by Peregrine (1967) and decimated ETOPO2 bathymetry along the transect (Fig. 11c).

For small values of $\tau$ (e.g., 20 sec), tsunami evolution proceeds in a standard manner, where the tsunami splits from the source region (Fig. 11b, black), with each outgoing wave decreasing to approximately half its initial amplitude (Fig. 11d). For longer values of $\tau$ (1000 sec and 1 hr), the tsunami waves leave the source region before generation is completed, such that the overall amplitude of the outgoing waves is reduced. There is also a lag in the leading phases for the eastward (depression) and westward (elevation) propagating waves for the $\tau = 1000$ sec case in comparison to $\tau = 20$ sec (red and black arrows, Fig. 11b). In contrast to the $\tau = 20$ sec case, there is little reduction in amplitude as the waves leave the source region for longer values of $\tau$, indicating that for these large values of $\tau$, tsunami generation is more sensitive to the time history of movement than details of the initial vertical displacement profile (cf., Hammack, 1973). Thus, afterslip with an exponential time constant less than 1 hr probably has a significant contribution to tsunami amplitude. A two-stage slip evolution description might be most reasonable, in which normal seismic rise times are followed by a physical afterslip model (e.g., Hashimoto *et al.*, 2006). Such a model would correspond to brittle failure followed by creeplike deformation as originally proposed for tsunami generation by Kanamori (1972). For tsunami assessment purposes, however, more information is needed to quantify temporal afterslip than is currently available for most subduction zones.

## Discussion

The objective of this study has been to test current methods of tsunami forecasting and assessment against a variety of observations of the 2004 Indian Ocean tsunami. Simple scalar, point-source empirical relationships can be used to estimate mean and maximum tsunami amplitudes once the seismic moment is known. These relationships provide a quick estimate of tsunami amplitudes and, as tested against tsunami observations from the 2004 Sumatra–Andaman earthquake, are fairly accurate except at sites along the main beam of tsunami energy. Tsunami forecasting using a combination of a subfault characterization of earthquake rupture with slip constrained by real-time deep-ocean tsunami measurements, appears to perform well in hindcasts of regional tsunami amplitudes, travel times, and inundation at Banda Aceh. For this hindcast, satellite altimetry measurements are

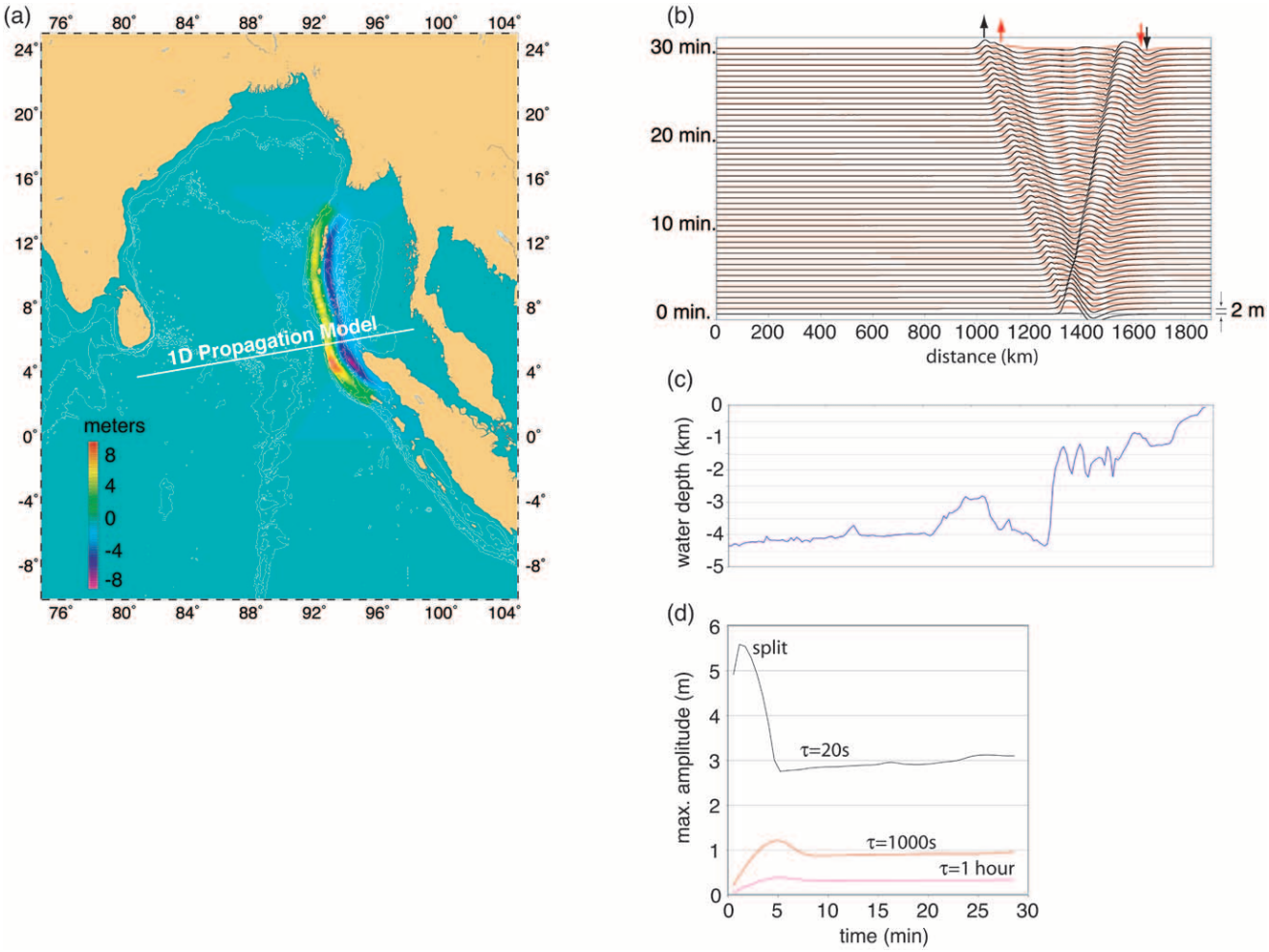


Figure 11. Sensitivity of tsunami generation to slip evolution on the fault. (a) Map showing 1D transect across vertical displacement field for slip distribution shown in Figure 8a. (b) Evolution of tsunami waveforms propagating outward from the source for $\tau = 20$ sec (black) and $\tau = 1000$ sec (red). Propagation time increases from $t = 0$ (bottom) to $t = 30$ min (top). Each horizontal line represents 2 m in amplitude. Arrows indicate position of leading phases after 30 min. (c) Bathymetry along transect. (d) Maximum tsunami amplitude as a function of time for three different values of exponential time constant $\tau$.

substituted for tsunami time series from DART stations to constrain the seismic source.

For tsunami assessments, one typically must first assign a maximum credible magnitude to the study region. Before the 26 December 2004 earthquake, it is unclear whether a tsunami assessment for the Sumatra–Andaman interplate thrust would have been based on an earthquake as large as $M_w$ 9.0–9.3. For future assessments, therefore, it may be prudent to adopt the conclusion of Bird and Kagan (2004) that all interplate thrusts are capable of producing great earthquakes (given that the fault is long enough), unless proven otherwise.

Using end-member cases for average slip and rupture length relative to a $M_w$ 9.0–9.3 earthquake, we determine how uncertainty in first-order source parameters affect tsunami assessments. On the one hand, high slip values are needed to explain extreme runup in the western Aceh Province (as well as the direct arrival from the this region of slip observed in the Jason-1 data). However, using a high average slip value will overpredict tsunami runup elsewhere, particularly in Myanmar. Reducing the fault length only partially compensates for increased runup in the northern part of the study area.

One explanation for this paradox is that slip is significantly more heterogeneous for this earthquake than slip models used in Geist (2002, 2005). The degree of slip heterogeneity can be approximated by comparing maximum slip ($u_{max}$) with average slip ($\bar{u}$). For the stochastic slip model, $u_{max}/\bar{u}$ is approximately 2 and is consistent with observed ratios for previous $M$ <8.5 earthquakes (e.g., Manighetti *et al.*, 2005). In constrast, $u_{max}/\bar{u} \geq 3$ for the 2004 Sumatra–Anadman earthquake from many of the source in-

versions (e.g., Fujii and Satake, 2007). For the 1957 Aleutian earthquake, $u_{max}/\bar{u}$ is also quite large ($\geq$4) (Johnson and Satake, 1993). It is unlikely that the difference in slip heterogeneity is specific to $M > 9$ earthquakes, though, since the maximum/average slip ratio for the 1964 Alaska earthquake is approximately 2 (Johnson *et al.*, 1996), suggesting self-similarity with smaller earthquakes. Lavallée and Archuleta (2003) and Lavallée *et al.* (2006) recently indicate that stochastic slip models based on Gaussian random variables may not fully account for the spatial variability of slip. Instead, Lavallée *et al.* (2006) suggest that the Lévy probability law in general better captures extreme values of slip for a given earthquake. Further research is needed to explain why some earthquakes such as the 2004 Sumatra–Andaman event seem to be characterized by large fluctuations in slip.

What is clear from this and previous tsunami assessment models is that uncertainty in first-order source parameters such as rupture length and slip-length scaling leads to significant, but quantifiable, uncertainty in tsunami amplitudes, particularly at local and regional distances. Uncertainty in slip distribution patterns also has a significant effect on local tsunamis, as does the rupture mechanics in the shallow subduction zones. These and other uncertainties can be incorporated into a probabilistic tsunami assessment (Lin and Tung, 1982; Ward, 2002; Geist and Parsons, 2006) using an approach similar to probabilistic seismic hazard analysis. From a probabilistic perspective, the uncertainty in slip-length scaling and the uncertainty expressed by slip heterogeneity can be considered sources of epistemic and aleatory uncertainty, respectively, although the two may not be independent as suggested by Zeng *et al.* (2005). Because the hydrodynamics of runup and inundation critically depend on high-resolution digital elevation models and computationally intensive nonlinear calculations, incorporating any level of source uncertainty into probabilistic assessment of tsunami hazards has only been recently attempted (Tsunami Pilot Study Working Group, 2006). Computationally efficient threshold modeling is a technique where effects of a wide range of source-parameter variation on tsunami amplitudes can be examined, prior to detailed inundation studies or where the nearshore bathymetric data is unavailable.

## Conclusions

Different earthquake parameterizations as implemented in tsunami generation models have been tested against observations from the 26 December 2004 Indian Ocean tsunami. For forecast models, simple scalar tsunami estimates from the seismic moment of the earthquake yield a surprisingly good match to the observed mean regional runup and maximum local runup, but a poorer match to regional tsunami runup heights on an azimuth in line with the tsunami beaming pattern. While the empirical relations do not rely on numerical modeling or higher-order parameterization of the earthquake, there is significant uncertainty and no site response associated with these estimates. The tsunami forecast model implemented in the Pacific Ocean uses a static subfault representation of earthquake rupture and real-time sea level observations to constrain slip on the subfaults. In place of time series of deep-ocean tsunami amplitudes at specific points, a transect of deep-ocean tsunami amplitudes recorded by satellite altimetry were used to constrain slip on four subfaults for the Sumatra–Andaman rupture. This proxy appears to perform well in comparison to observed regional tsunami amplitudes, travel times, and inundation patterns at Banda Aceh.

Tsunami assessments based on an $M_w$ 9.0–9.3 earthquake were compared, using end-member values for both average slip and rupture length. The linear propagation model is adequate for performing such a comparison of tsunami amplitude produced by different source parameters, although it should be emphasized that a detailed tsunami hazard assessment for a particular site requires high-resolution bathymetry and nonlinear runup and inundation computations. Average slip values in line with several seismic, geodetic, and tsunami inversions are consistent with most runup observations following the 2004 Sumatra–Andaman earthquake, except near the region of high slip in the southern part of the rupture. Peak slip, higher than what is expected from standard stochastic slip distributions, is needed to explain the extreme runup values in western Aceh Province and the direct arrival observed on the Jason-1 altimetry profile. Although estimation of peak slip is a critical parameter, especially for estimating local tsunami runup, it is unclear under what conditions great earthquakes may result in large fluctuations of slip.

## Acknowledgments

The authors appreciate inversion results for the 2004 Sumatra–Andaman earthquake generously provided by Mohamed Chlieh, Chen Ji, and Hong Kie Thio. This article greatly benefited from constructive reviews by Tom Parsons, Paul Whitmore, Barry Hirshorn, guest editor Kenji Satake, and an anonymous reviewer. Some maps were created using Generic Mapping Tools software (Wessel and Smith, 1995).

## References

Abe, K. (1979). Size of great earthquake of 1837–1974 inferred from tsunami data, *J. Geophys. Res.* **84,** 1561–1568.

Abe, K. (1981). Physical size of tsunamigenic earthquakes of the northwestern Pacific, *Phys. Earth Planet. Interiors* **27,** 194–205.

Abe, K. (1995). Estimate of tsunami run-up heights from earthquake magnitudes, in *Tsunami: Progress in Prediction, Disaster Prevention and Warning*, Y. Tsuchiya and N. Shuto (Editors), Kluwer Academic Publishers, Dordrecht, pp. 21–35.

Ammon, C. J., C. Ji, H. K. Thio, D. Robinson, S. Ni, V. Hjorleifsdottir, H. Kanamori, T. Lay, S. Das, D. Helmberger, G. Ichinose, J. Polet, and D. Wald (2005). Rupture process of the 2004 Sumatra-Andaman earthquake, *Science* **308,** 1133–1139.

Andrews, D. J. (1980). A stochastic fault model 1. Static case, *J. Geophys. Res.* **85,** 3867–3877.

Banerjee, P., F. F. Pollitz, and R. Bürgmann (2005). The size and duration of the Sumatra–Andaman earthquake from far-field static offsets, *Science* **308,** 1769–1772.

Banerjee, P., F. F. Pollitz, B. Nagarajan, and R. Bürgmann (2007). Coseismic slip distributions of the 26 December 2004 Sumatra–Andaman and 28 March 2005 Nias earthquake from GPS static offsets, *Bull. Seism. Soc. Am.* **97,** no. 1A, S86–S102.

Ben-Menahem, A., and M. Rosenman (1972). Amplitude patterns of tsunami waves from submarine earthquakes, *J. Geophys. Res.* **77,** 3097–3128.

Ben-Zion, Y., and J. R. Rice (1995). Slip patterns and earthquake populations along different classes of faults in elastic solids, *J. Geophys. Res.* **100,** 12,959–12,983.

Ben-Zion, Y., and J. R. Rice (1997). Dynamic simulations of slip on a smooth fault in an elastic solid, *J. Geophys. Res.* **102,** 17,771–17,784.

Berge, C., J. C. Gariel, and P. Bernard (1998). A very broad-band stochastic source model used for near source strong motion prediction, *Geophys. Res. Lett.* **25,** 1063–1066.

Bilek, S. L. (2007). Using earthquake rupture variations along the Sumatra–Andaman subduction system to examine fault zone variations, *Bull. Seism. Soc. Am.* **97,** no. 1A, S62–S70.

Bilek, S. L., and T. Lay (1999). Rigidity variations with depth along interplate megathrust faults in subduction zones, *Nature* **400,** 443–446.

Bilek, S. L., and T. Lay (2000). Depth dependent rupture properties in circum-Pacific subduction zones, in *GeoComplexity and the Physics of Earthquakes*, J. B. Rundle, D. L. Turcotte, and W. Klein (Editors), American Geophysical Union, Washington, D.C., pp. 165–186.

Bilek, S. L., and T. Lay (2002). Tsunami earthquakes possibly widespread manifestations of frictional conditional stability, *Geophys. Res. Lett.* **29,** doi 10.1029/2002GL015215.

Bilek, S. L., S. Y. Schwartz, and H. R. DeShon (2003). Control on seafloor roughness on earthquake rupture behaviour, *Geology* **31,** 455–458.

Bird, P. (2003). An updated digital model of plate boundaries, *Geochem. Geophys. Geosystems* **4,** doi 10.1029/2001GC000252.

Bird, P., and Y. Y. Kagan (2004). Plate-tectonic analysis of shallow seismicity: apparent boundary width, beta-value, corner magnitude, coupled lithosphere thickness, and coupling in 7 tectonic settings, *Bull. Seism. Soc. Am.* **94,** 2380–2399.

Borrero, J. C. (2005). Field survey of northern Sumatra and Banda Aceh, Indonesia after the tsunami and earthquake of 26 December 2004, *Seism. Res. Lett.* **76,** 312–320.

Boyd, T. M., E. R. Engdahl, and W. Spence (1995). Seismic cylces along the Aleutian arc: analysis of seismicity from 1957 through 1991, *J. Geophys. Res.* **100,** 621–644.

Chlieh, M., J. P. Avouac, V. Hjorleifsdottir, T. A. Song, C. Ji, K. Sieh, A. Sladen, H. Hebert, L. Prawirodirdjo, Y. Bock, and J. Galetzka (2007). Coseismic slip and afterslip of the great ($M_w$ 9.15) Sumatra–Andaman earthquake of 2004, *Bull. Seism. Soc. Am.* **97,** no. 1A, S152–S173.

Cifuentes, I. L. (1995). Seismic moment and duration of recent large and great earthquakes, *J. Geophys. Res.* **100,** no. 20, 3030–3020, 3309.

Comer, R. P. (1980). Tsunami height and earthquake magnitude: theoretical basis of an empirical relation, *Geophys. Res. Lett.* **7,** 445–448.

Das, S. (1988). Relation between average slip and average stress drop for rectangular faults with multiple asperities, *Bull. Seism. Soc. Am.* **78,** 924–930.

Dasgupta, S., and M. Mukhopadhyay (1993). Seismicity and plate deformation below the Andaman arc, northeastern Indian Ocean, *Tectonophysics* **225,** 529–542.

de Groot-Hedlin, C. D. (2005). Estimation of the rupture length and velocity of the Great Sumatra earthquake of Dec. 26, 2004 using hydroacoustic signals, *Geophys. Res. Lett.* **32,** doi 10.1029/2005GL022695.

Dmowska, R., and B. V. Kostrov (1973). A shearing crack in a semi-space under plane strain conditions, *Arch. Mech.* **25,** 421–440.

Fauzi, R. M., R. McCaffrey, D. Wark, D. Sunaryo, and P. Y. Prih Haryadi (1996). Lateral variation in slab orientation beneath Toba Caldera, northern Sumatra, *Geophys. Res. Lett.* **23,** 443–446.

Fitch, T. J. (1972). Plate convergence, transcurrent faults, and internal deformation adjacent to southeast Asia and the western Pacific, *J. Geophys. Res.* **77,** 4432–4460.

Fu, G., and W. Sun (2004). Effects of spatial distribution of fault slip on calculating coseismic displacement: case studies of the Chi-Chi earthquake ($M_w$ 7.6) and the Kunlun earthquake ($M_w$ 7.8), *Geophys. Res. Lett.* **31,** doi 10.1029/2004GL020841.

Fujii, Y., and K. Satake (2007). Tsunami source of the 2004 Sumatra–Andaman earthquake inferred from tide gauge and satellite data, *Bull. Seism. Soc. Am.* **97,** no. 1A, S192–S207.

Fujima, K., D. Yuliadi, C. Goto, K. Hayashi, and T. Shigemura (1995). Characteristics of long wave trapped by conical island, *Coastal Eng. Jpn.* **38,** 111–132.

Furumoto, A. S. (1996). Using Mw or Mt to forecast tsunami heights, *Sci. Tsunami Haz.* **14,** 107–118.

Geist, E. L. (1999). Local tsunamis and earthquake source parameters, *Adv. Geophys.* **39,** 117–209.

Geist, E. L. (2002). Complex earthquake rupture and local tsunamis, *J. Geophys. Res.* **107,** doi 10.1029/2000JB000139.

Geist, E. L. (2005). Local tsunami hazards in the Pacific Northwest from Cascadia Subduction Zone earthquakes, *U.S. Geol. Surv. Profess. Pap. 1661B*, 17 pp.

Geist, E. L., and S. L. Bilek (2001). Effect of depth-dependent shear modulus on tsunami generation along subduction zones, *Geophys. Res. Lett.* **28,** 1315–1318.

Geist, E. L., and R. Dmowska (1999). Local tsunamis and distributed slip at the source, *Pure Appl. Geophys.* **154,** 485–512.

Geist, E. L., and T. Parsons (2006). Probabilistic analysis of tsunami hazards, *Nat. Haz.* **37,** 277–314.

Geist, E. L., and S. Yoshioka (1996). Source parameters controlling the generation and propagation of potential local tsunamis along the Cascadia margin, *Nat. Haz.* **13,** 151–177.

Geist, E. L., S. L. Bilek, D. Arcas, and V. V. Titov (2006). Differences in tsunami generation between the 26 December 2004 and 28 March 2005 Sumatra earthquakes, *Earth Planets Space* **58,** 185–193.

Geller, R. J. (1976). Scaling relations for earthquake source parameters and magnitudes, *Bull. Seism. Soc. Am.* **66,** 1501–1523.

Genrich, J. F., Y. Bock, R. McCaffrey, L. Prawirodirdjo, C. W. Stevens, S. S. O. Puntodewo, C. Subarya, and S. Wdowinski (2000). Distribution of slip at the northern Sumatran fault system, *J. Geophys. Res.* **105,** 28,327–28,341.

Goff, J. R., P. L. F. Liu, B. Higman, R. Morton, B. E. Jaffe, H. Fernando, P. Lynett, H. M. Fritz, C. E. Synolakis, and S. Fernando (2006). Sri Lanka Field Survey after the December 2004 Indian Ocean tsunami, *Earthquake Spectra* **22,** S155–S172.

González, F. I., V. V. Titov, H. O. Mofjeld, A. J. Venturato, S. Simmons, R. Hansen, R. A. Combellick, R. K. Eisner, D. Hoirup, B. Yanagi, S. Yong, M. Darienzo, G. R. Priest, G. Crawford, and T. Walsh (2005). Progress in NTHMP hazard assessment, *Nat. Haz.* **35,** 89–110.

Gower, J. (2005). Jason 1 detects the 26 December 2004 tsunami, *EOS Trans. AGU* **86,** 37–38.

Gudmundsson, O., and M. Sambridge (1998). A regionalized upper mantle (RUM) seismic model, *J. Geophys. Res.* **103,** 7121–7136.

Hammack, J. L. (1973). A note on tsunamis: their generation and propagation in an ocean of uniform depth, *J. Fluid Mech.* **60,** 769–799.

Hanson, J. A., and J. R. Bowman (2005). Dispersive and reflected tsunami signals from the 2004 Indian Ocean tsunami observed on hydrophones and seismic stations, *Geophys. Res. Lett.* **32,** doi 10.1029/2005GL023783.

Hashimoto, M., N. Choosakul, M. Hashizume, S. Takemoto, H. Takiguchi, Y. Fukuda, and K. Fujimore (2006). Crustal deformations associated with the great Sumatra–Andaman earthquake deduced from continuous GPS observation, *Earth Planets Space* **58,** 127–139.

Heki, K., and Y. Tamura (1997). Short term afterslip in the 1994 Sanriku-Haruka-Oki earthquake, *Geophys. Res. Lett.* **24,** 3285–3288.

Herrero, A., and P. Bernard (1994). A kinematic self-similar rupture process for earthquakes, *Bull. Seism. Soc. Am.* **84,** 1216–1228.

Hirata, K., K. Satake, Y. Tanioka, T. Kuragano, Y. Hasegawa, Y. Hayashi, and M. Hamada (2006). The 2004 Indian Ocean tsunami: tsunami source model from satellite altimetry, *Earth Planets Space* **58,** 195–201.

Hirata, K., Y. Tanioka, K. Satake, S. Yamaki, and E. L. Geist (2004). The tsunami source area of the 2003 Tokachi-oki earthquake estimated from tsunami travel times and its relationship to the 1952 Tokachi-oki earthquake, *Earth Planets Space* **56,** 367–372.

Hisada, Y. (2000). A theoretical omega-square model considering the spatial variation in slip and rupture velocity, *Bull. Seism. Soc. Am.* **90,** 387–400.

Hisada, Y. (2001). A theoretical omega-square model considering the spatial variation in slip and rupture velocity, part 2: Case for a two-dimensional source model, *Bull. Seism. Soc. Am.* **91,** 651–666.

Honda, R., and K. Yomogida (2003). Effect of complex fault geometry and slip style on near-fault strong motions and static displacment, *Earth Planets Space* **55,** 515–530.

Honda, S., and T. Seno (1989). Seismic moment tensors and source depths determined by the simultaneous inversion of body and surface waves, *Phys. Earth Planet. Interiors* **57,** 311–329.

Ishii, M., P. M. Shearer, H. Houston, and J. E. Vidale (2005). Extent, duration and speed of the 2004 Sumatra–Andaman earthquake imaged by the Hi-Net array, *Nature* **435,** 933–936.

Jaffe, B. E., J. C. Borrero, G. S. Prasetya, R. Peters, B. McAdoo, G. Gelfenbaum, R. Morton, P. Ruggiero, B. Higman, L. Dengler, R. Hidayat, E. Kingsley, W. Kongko, Lukijanto, A. Moore, V. V. Titov, and E. Yulianto (2006). Northwest Sumatra and Offshore Islands Field Survey after the December 2004 Indian Ocean tsunami, *Earthquake Spectra* **22,** S105–S135.

Jain, S. K., C. V. R. Murty, D. C. Rai, J. N. Malik, A. R. Sheth, A. Jaiswal, S. A. Sanyal, H. B. Kaushik, P. Gandhi, G. Mondal, S. R. Dash, J. S. Sodhi, and G. S. Kumar (2005). The great Sumatra Earthquake and Indian Ocean tsunami of December 26, 2004, Report 3: The effects in mainland India and in the Andaman-Nicobar Islands, EERI Special Earthquake Report, April 2005, 1–12.

Johnson, J. M., and K. Satake (1993). Source parameters of the 1957 Aleutian earthquake from tsunami waveforms, *Geophys. Res. Lett.* **20,** 1487–1490.

Johnson, J. M., K. Satake, S. R. Holdahl, and J. Sauber (1996). The 1964 Prince William Sound earthquake: Joint inversion of tsunami and geodetic data, *J. Geophys. Res.* **101,** 523–532.

Kagan, Y. Y. (2002). Seismic moment distribution revisited: II. Moment conservation principle, *Geophys. J. Int.* **149,** 731–754.

Kajiura, K. (1981). Tsunami energy in relation to parameters of the earthquake fault model, *Bull. Earthquake Res. Ins.* **56,** 415–440.

Kanamori, H. (1972). Mechanism of tsunami earthquakes, *Phys. Earth Planet. Interiors* **6,** 346–359.

Kanamori, H., and D. L. Anderson (1975). Theoretical basis of some empirical relations in seismology, *Bull. Seism. Soc. Am.* **65,** 1073–1095.

Karig, D. E., G. F. Moore, J. R. Curray, and M. B. Lawrence (1980). Morphology and shallow structure of the lower trench slope off Nias Island, Sunda Arc, in *The Tectonic and Geologic Evolution of Southeast Asian Seas and Islands*, D. E. Hayes (Editor), American Geophysical Monograph 23, 179–208.

Kato, T., and M. Ando (1997). Source mechanisms of the 1944 Tonankai and 1946 Nankaido earthquakes: spatial heterogeneity of rise times, *Geophys. Res. Lett.* **24,** 2055–2058.

Kawakatsu, H., and G. P. Cadena (1991). Focal mechanisms of the March 6, 1987 Ecuador earthquakes—CMT inversion with a first motion constraint, *J. Phys. Earth* **39,** 589–597.

Kikuchi, M., and H. Kanamori (1995). Source characteristics of the 1992 Nicaragua tsunami earthquake inferred from teleseismic body waves, *Pure Appl. Geophys.* **144,** 441–453.

Kikuchi, M., H. Kanamori, and K. Satake (1993). Source complexity of the 1988 Armenian earthquake: evidence for a slow after-slip event, *J. Geophys. Res.* **98,** 15,797–15,808.

Koshimura, S., F. Imamura, and N. Shuto (1999). Propagation of obliquely incident tsunamis on a slope, Part I: Amplification of tsunamis on a continental slope, *Coastal Eng. J.* **41,** 151–164.

Kowalik, Z., W. Knight, T. Logan, and P. Whitmore (2005). Numerical modeling of the global tsunami: Indonesian Tsunami of 26 December 2004, *Sci. Tsunami Haz.* **23,** 40–56.

Krishna, M. R., and T. D. Sanu (2002). Shallow seismicity, stress distribution and crustal deformation pattern in the Andaman–West Sunda arc and Andaman Sea, northeastern Indian Ocean, *J. Seism.* **6,** 25–41.

Krüger, F., and M. Ohrnberger (2005). Tracking the rupture of the Mw = 9.3 Sumatra earthquake over 1,150 km at teleseismic distance, *Nature* **435,** 937–939.

Lavallée, D., and R. J. Archuleta (2003). Stochastic modeling of slip spatial complexities for the 1979 Imperial Valley, California, earthquake, *Geophys. Res. Lett.* **30,** doi 10.1029/2002GL015839.

Lavallée, D., P. Liu, and R. J. Archuleta (2006). Stochastic model of heterogeneity in earthquake slip spatial distributions, *Geophys. J. Int.* **165,** 622–640.

Lay, T., H. Kanamori, C. J. Ammon, M. Nettles, S. N. Ward, R. C. Aster, S. L. Beck, S. L. Bilek, M. R. Brudzinski, R. Butler, H. R. DeShon, G. Ekström, K. Satake, and S. A. Sipkin (2005). The great Sumatra–Andaman earthquake of 26 December 2004, *Science* **308,** 1127–1133.

Lin, I., and C. C. Tung (1982). A preliminary investigation of tsunami hazard, *Bull. Seism. Soc. Am.* **72,** 2323–2337.

Liu, P. L. F., P. Lynett, H. Fernando, B. E. Jaffe, H. M. Fritz, B. Higman, R. Morton, J. R. Goff, and C. E. Synolakis (2005). Observations by the International Tsunami Survey Team in Sri Lanka, *Science* **308,** 1595.

Liu, P. L. F., H. Yeh, P. Lin, K. T. Chang, and Y. S. Cho (1998). Generation and evolution of edge-wave packets, *Phys. Fluids* **10,** 1635–1657.

Mai, P. M., and G. C. Beroza (2002). A spatial random field model to characterize complexity in earthquake slip, *J. Geophys. Res.* **107,** doi 10.1029/2001JB000588.

Manighetti, I., M. Campillo, C. Sammis, P. M. Mai, and G. King (2005). Evidence for self-similar, triangular slip distributions on earthquakes: implications for earthquake and fault mechanics, *J. Geophys. Res.* **110,** doi 10.1029/2004JB003174.

Maung, H. (1987). Trancurrent movements in the Burma-Andaman Sea region, *Geology* **15,** 911–912.

Mazzotti, S., X. Le Pichon, P. Henry, and S. Miyazaki (2000). Full interseismic locking of the Nankai and Japan-west Kurile subduction zones: an analysis of uniform elastic strain accumulation in Japan constrained by permanent GPS, *J. Geophys. Res.* **105,** 13,159–13,177.

McCaffrey, R. (1991). Slip vectors and stretching of the Sumatran fore arc, *Geology* **19,** 881–884.

McCaffrey, R. (1992). Oblique plate convergence, slip vectors, and forearc deformation, *J. Geophys. Res.* **97,** 8905–8915.

McCaffrey, R. (1997). Influences of recurrence times and fault zone temperatures on the age-rate dependence of subduction zone seismicity, *J. Geophys. Res.* **102,** 22,839–22,854.

McCaffrey, R., P. C. Zwick, Y. Bock, L. Prawirodirdjo, J. F. Genrich, C. W. Stevens, S. S. O. Puntodewo, and C. Subarya (2000). Strain partitioning during oblique plate convergence in northern Sumatra: Geodetic and seismologic constraints and numerical modeling, *J. Geophys. Res.* **105,** 28,363–28,376.

McGarr, A., and J. B. Fletcher (2003). Maximum slip in earthquake fault zones, apparent stress, and stick-slip friction, *Bull. Seism. Soc. Am.* **93,** 2355–2362.

McGuire, J. J., L. Zhao, and T. H. Jordan (2001). Teleseismic inversion for the second-degree moments of earthquake space-time distributions, *Geophys. J. Int.* **145,** 661–678.

Mei, C. C. (1989). *The Applied Dynamics of Ocean Surface Waves*, World Scientific, Singapore, 740 pp.

Meltzner, A., K. Sieh, M. Abrams, D. C. Agnew, K. W. Hudnut, J. P. Avouac, and D. Natawidjaja (2006). Uplift and subsidence associated with the Great Aceh-Andaman earthquake of 2004, *J. Geophys. Res.* **111,** doi 10.1029/2005JB003891.

Mendoza, C. (1993). Coseismic slip of two large Mexican earthquakes from teleseismic body waveforms: implications for asperity interaction in the Michoacan plate boundary segment, *J. Geophys. Res.* **98,** 8197–8210.

Michael, A. J., and R. J. Geller (1984). Linear moment tensor inversion for

shallow thrust earthquakes combining first-motion and surface wave data, *J. Geophys. Res.* **89,** 1889–1897.

Michel, G. W., M. Becker, C. Reigber, R. Tibi, Y. Q. Yu, and S. Y. Zhu (2001). Regional GPS data confirm high strain accumulation prior to the 2000 June 4 Mw = 7.8 earthquake at southeast Sumatra, *Geophys. J. Int.* **146,** 571–582.

Miyazaki, S., K. M. Larson, K. Choi, K. Hikima, K. Koketsu, P. Bodin, J. Haase, G. Emore, and A. Yamagiwa (2004). Modeling the rupture process of the 2003 September 25 Tokachi-Oki (Hokkaido) earthquake using 1-Hz GPS data, *Geophys. Res. Lett.* **31,** doi 10.1029/2004GL021457.

Moore, G. F., J. R. Curray, D. G. Moore, and D. E. Karig (1980). Variations in geologic structure along the Sunda fore arc, northeastern Indian Ocean, in *The Tectonic and Geologic Evolution of Southeast Asian Seas and Islands*, D. E. Hayes (Editor), American Geophysical Monograph 23, 145–160.

Mukhopadhyay, M. (1984). Seismotectonics of subduction and back-arc rifting under the Andaman Sea, *Tectonophysics* **108,** 229–239.

Neetu, S., I. Suresh, R. Shankar, D. Shankar, S. S. C. Shenoi, S. R. Shetye, D. Sundar, and B. Nagarajan (2005). Comment on "The Great Sumatra-Andaman Earthquake of 26 December 2004," *Science* **310,** 1431.

Newcomb, K. R., and W. R. McCann (1987). Seismic history and seismotectonics of the Sunda arc, *J. Geophys. Res.* **92,** 421–439.

Ni, S., H. Kanamori, and D. Helmberger (2005). Energy radiation from the Sumatra earthquake, *Nature* **434,** 582.

Nielsen, S. B., and J. M. Carlson (2000). Rupture pulse characterization: self-healing, self-similar, expanding solutions in a continuum model of fault dynamics, *Bull. Seism. Soc. Am.* **90,** 1480–1497.

Okada, Y. (1985). Surface deformation due to shear and tensile faults in a half-space, *Bull. Seism. Soc. Am.* **75,** 1135–1154.

Okal, E. A. (1988). Seismic parameters controlling far-field tsunami amplitudes: a review, *Nat. Haz.* **1,** 67–96.

Okal, E. A. (1991). Erratum. Seismic parameters controlling far-field tsunami amplitudes: a review, *Nat. Haz.* **4,** 433.

Okal, E. A., and C. E. Synolakis (2004). Source discriminants for near-field tsunamis, *Geophys. J. Int.* **158,** 899–912.

Ortiz, M., and R. Bilham (2003). Source area and rupture parameters of the 31 December 1881 Mw = 7.9 Car Nicobar earthquake estimated from tsunamis recorded in the Bay of Bengal, *J. Geophys. Res.* **108,** doi 10.1029/2002JB001941.

Park, J., T. A. Song, J. Tromp, E. A. Okal, S. Stein, G. Roult, E. Clevede, G. Laske, H. Kanamori, P. Davis, J. Berger, C. Braitenberg, M. Van Camp, X. Lei, H. Sun, H. Xu, and S. Rosat (2005). Earth's free oscillations excited bythe 26 December 2004 Sumatra–Andaman earthquake, *Science* **308,** 1139–1144.

Paul, J., R. Bürgmann, V. K. Gaur, R. Bilham, K. M. Larson, M. B. Ananda, S. Jade, M. Mukal, T. S. Anupama, G. Satyal, and D. Kumar (2000). The motion and active deformation of India, *Geophys. Res. Lett.* **28,** 647–650.

Pelayo, A. M., and D. A. Wiens (1992). Tsunami earthquakes: slow thrust-faulting events in the accretionary wedge, *J. Geophys. Res.* **97,** 15,321–15,337.

Peregrine, D. H. (1967). Long waves on a beach, *J. Fluid Mech.* **27,** 815–827.

Perfettini, H., J. Schmittbuhl, and J. P. Vilotte (2001). Slip correlations on a creeping fault, *Geophys. Res. Lett.* **28,** 2137–2140.

Polet, J., and H. Kanamori (2000). Shallow subduction zone earthquakes and their tsunamigenic potential, *Geophys. J. Int.* **142,** 684–702.

Pollitz, F. F. (1996). Coseismic deformation from earthquake faulting on a layered spherical earth, *Geophys. J. Int.* **125,** 1–14.

Prawirodirdjo, L., Y. Bock, R. McCaffrey, J. F. Genrich, E. Calais, C. W. Stevens, S. S. O. Puntodewo, C. Subarya, J. Rais, P. C. Zwick, and R. M. Fauzi (1997). Geodetic observations of interseismic strain segmentation at the Sumatra subduction zone, *Geophys. Res. Lett.* **24,** 2601–2604.

Rabinovich, A. B. (1997). Spectral analysis of tsunami waves: separation of source and topography effects, *J. Geophys. Res.* **102,** 12,663–12,676.

Reid, R. O., and B. R. Bodine (1968). Numerical model for storm surges in Galveston Bay, *J. Waterways Harbors Div. A.C.E.* **94,** 33–57.

Rikitake, T., and I. Aida (1988). Tsunami hazard probability in Japan, *Bull. Seism. Soc. Am.* **78,** 1268–1278.

Romanowicz, B., and J. B. Rundle (1993). On scaling relationships for large earthquakes, *Bull. Seism. Soc. Am.* **83,** 1294–1297.

Rudnicki, J. W., and M. Wu (1995). Mechanics of dip-slip faulting in an elastic half-space, *J. Geophys. Res.* **100,** 22,173–22,186.

Satake, K. (1995). Linear and nonlinear computations of the 1992 Nicaragua earthquake tsunami, *Pure Appl. Geophys.* **144,** 455–470.

Satake, K. (2002). Tsunamis, in *International Handbook of Earthquake and Engineering Seismology, Part A*, W. H. K. Lee, H. Kanamori, P. C. Jennings and C. Kisslinger (Editors) Academic Press, San Diego, 437–451.

Satake, K., and H. Kanamori (1991). Use of tsunami waveforms for earthquake source study, *Nat. Haz.* **4,** 193–208.

Satake, K., T. T. Aung, Y. Sawai, Y. Okamura, K. S. Win, W. Swe, C. Swe, T. L. Swe, S. T. Tun, M. M. Soe, T. Z. Oo, and S. H. Zaw (2006b). Tsunami heights and damage along the Myanmar coast from the December 26 Sumatra-Andaman earthquake, *Earth Planets Space* **58,** 243–252.

Satake, K., K. Hirata, S. Yamaki, and Y. Tanioka (2006a). Re-estimation of tsunami source of the 1952 Tokachi-oki earthquake, *Earth Planets Space* **58,** 535–542.

Satake, K., K. Wang, and B. F. Atwater (2003). Fault slip and seismic moment of the 1700 Cascadia earthquake inferred from Japanese tsunami descriptions, *J. Geophys. Res.* **108,** ESE.7-1–7-17.

Scholz, C. H. (1982). Scaling laws for large earthquakes: consequences for physical models, *Bull. Seism. Soc. Am.* **72,** 1–14.

Scholz, C. H. (1994). A reappraisal of large earthquake scaling, *Bull. Seism. Soc. Am.* **84,** 215–218.

Schwartz, S. Y. (1999). Noncharacteristic behavior and complex recurrence of large subduction zone earthquakes, *J. Geophys. Res.* **104,** 23,111–23,125.

Seno, T., and K. Hirata (2007). Is the 2004 Sumatra–Andaman earthquake a tsunami earthquake? *Bull. Seism. Soc. Am.* **97,** no. 1A, S296–S306.

Shaw, B. E. (2004). Dynamic heterogeneities versus fixed heterogeneities in earthquake models, *Geophys. J. Int.* **156,** 275–286.

Shibata, M. (1983). One-dimensional dispersive deformation of tsunami with typical inital profiles on continental topographies, in *Tsunamis: Their Science and Engineering*, K. Iida and T. Iwasaki (Editors), Terra Science Publication Company, Tokyo, 241–250.

Shuto, N. (1991). Numerical simulation of tsunamis—its present and near future, *Nat. Haz.* **4,** 171–191.

Sieh, K., R. Briggs, A. Meltzner, D. Natawidjaja, N. Hananto, and I. Suprihanto (2005). The Simeulue saddle: evidence for a barrier to rupture for both the 2004 and 2005 Sumatran megathrust failures (abstract), *EOS Trans. AGU.* **86,** no. 52, Fall Meeting Suppl., abstract U14A-01.

Simons, W. M. F., B. A. C. Ambrosius, R. Noomen, D. Angermann, P. Wilson, M. Becker, E. Reinhard, A. Walpersdorf, and C. Vigny (1999). Observing plate motions in SE Asia: geodetic results of the GEODYSSEA project, *Geophys. Res. Lett.* **26,** 2081–2084.

Somerville, P., K. Irikura, R. Graves, S. Sawada, D. Wald, N. A. Abrahamson, Y. Iwasaki, T. Kagawa, N. Smith, and A. Kowada (1999). Characterizing crustal earthquake slip models for the prediction of strong ground motion, *Seism. Res. Lett.* **70,** 59–80.

Stein, S., and E. A. Okal (2005). Speed and size of the Sumatra earthquake, *Nature* **434,** 581–582.

Subarya, C., M. Chlieh, L. Prawirodirdjo, J. P. Avouac, Y. Bock, K. Sieh, A. Meltzner, D. Natawidjaja, and R. McCaffrey (2006). Plate-boundary deformation associated with the great Sumatra–Andaman earthquake, *Nature* **440,** 46–51.

Synolakis, C. E., and J. E. Skjelbreia (1993). Evolution of maximum amplitude of solitary waves on plane beaches, *J. Waterway Port Coastal Ocean Eng.* **119,** 323–342.

Tanioka, Y., and K. Satake (1996). Tsunami generation by horizontal displacement of ocean bottom, *Geophys. Res. Lett.* **23,** 861–865.

Tanioka, Y., L. J. Ruff, and K. Satake (1997). What controls the lateral variation of large earthquake occurrence along the Japan trench? *Island Arc* **6,** 261–266.

Tanioka, Y., Y. Yudhicara, T. Kususose, S. Kathiroli, Y. Nishimura, S. Iwasaki, and K. Satake (2006). Rupture process of the 2004 great Sumatra–Andaman earthquake estimate from tsunami waveforms, *Earth Planets Space* **58,** 203–209.

Thatcher, W. (1990). Order and diversity in the modes of circum-Pacific earthquake recurrence, *J. Geophys. Res.* **95,** 2609–2623.

Tinti, S., and A. Armigliato (2003). The use of scnarios to evaluate the tsunami impact in southern Italy, *Mar. Geol.* **199,** 221–243.

Titov, V. V., and F. I. González (1997). Implementation and testing of the method of splitting tsunami (MOST) model, NOAA Technical Memorandum, NOAA/PMEL, Seattle, Washington, 11 pp.

Titov, V. V., and C. E. Synolakis (1997). Extreme inundation flows during the Hokkaido-Nansei-Oki tsunami, *Geophys. Res. Lett.* **24,** 1315–1318.

Titov, V. V., and C. E. Synolakis (1998). Numerical modeling of tidal wave runup, *J. Waterway Port Coastal Ocean Eng.* **124,** 157–171.

Titov, V. V., F. I. González, E. N. Bernard, J. E. Ebel, H. O. Mofjeld, J. C. Newman, and A. J. Venturato (2005a). Real-time tsunami forecasting: challenges and solutions, *Nat. Haz.* **35,** 40–58.

Titov, V. V., H. O. Mofjeld, F. I. González, and J. C. Newman (1999). Offshore forecasting of Hawaiian tsunamis generated in Alaskan-Aleutian subduction zone, NOAA Technical Memorandum ERL, Pacific Marine Environmental Laboratory (PMEL), Seattle, Washington, 26 pp.

Titov, V. V., H. O. Mofjeld, F. I. González, and J. C. Newman (2001). Offshore forecasting of Alaskan tsunami in Hawaii, in *Tsunami Research at the End of a Critical Decade*, G. T. Hebenstreit (Editor), Kluwer Academic Publishers, Dordrecht, The Netherlands, 75–90.

Titov, V. V., A. B. Rabinovich, H. O. Mofjeld, R. Thomson, and F. I. González (2005b). The global reach of the 26 December 2004 Sumatra tsunami, *Science* **309,** 2045–2048.

Tolstoy, M., and D. R. Bohnenstiehl (2005). Hydroacoustic constraints on the rupture duration, length, and speed of the great Sumatra–Andaman earthquake, *Seism. Res. Lett.* **76,** 419–425.

Tsai, C. P. (1997). Slip, stress drop and ground motion of earthquakes: a view from the perspective of fractional Brownian motion, *Pure Appl. Geophys.* **149,** 689–706.

Tsai, V. C., M. Nettles, G. Ekström, and A. M. Dziewonski (2005). Multiple CMT source analysis of the 2004 Sumatra earthquake, *Geophys. Res. Lett.* **32,** doi 10.1029/2005GL023813.

Tsuboi, S. (1999). Application of Mwp to deep and teleseismic earthquakes, *Bull. Seism. Soc. Am.* **89,** 1345–1351.

Tsuboi, S. (2000). Application of Mwp to tsunami earthquake, *Geophys. Res. Lett.* **27,** 3105–3108.

Tsuboi, S., K. Abe, K. Takano, and Y. Yamanaka (1995). Rapid determination of Mw from broadband P waveforms, *Bull. Seism. Soc. Am.* **85,** 606–613.

Tsuji, Y., H. Matsutomi, Y. Tanioka, Y. Nishimura, T. Sakakiyama, T. Kamataki, Y. Murakami, A. Moore, and G. Gelfenbaum (2005). Distribution of the tsunami heights of the 2004 Sumatera tsunami in Banda Aceh measured by the Tsunami Survey Team, edited, University of Tokyo, http://www.eri.u-tokyo.ac.jp/namegaya/sumatera/surveylog/eindex.htm (last accessed January 2005).

Tsuji, Y., Y. Namegaya, H. Matsumoto, S. Iwasaki, W. Kanbua, M. Sriwichai, and V. Meesuk (2006). The 2004 Indian tsunami in Thailand: surveyed runup heights and tide gauge records, *Earth Planets Space* **58,** 223–232.

Tsunami Pilot Study Working Group (2006). Seaside, Oregon Tsunami Pilot Study—Modernization of FEMA Flood Hazard Maps, *U.S. Geol. Surv. Open-File Rep. 2006-1234,* http://pubs.usgs.gov/of/2006/1234.

Vigny, C., W. M. F. Simons, S. Abu, R. Bamphenyu, C. Satirapod, N. Choosakul, C. Subarya, A. Socquet, K. Omar, H. Z. Abidin, and B. A. C. Ambrosius (2005). Insight into the 2004 Sumatra-Andaman earthquake from GPS measurements in southeast Asia, *Nature* **436,** 201–206.

Ward, S. N. (1980). Relationships of tsunami generation and an earthquake source, *J. Phys. Earth* **28,** 441–474.

Ward, S. N. (1982a). On tsunami nucleation II. An instantaneous modulated line source, *Phys. Earth Planet. Interiors* **27,** 273–285.

Ward, S. N. (1982b). Earthquake mechanisms and tsunami generation: the Kurile Islands event of 13 October 1963, *Bull. Seism. Soc. Am.* **72,** 759–777.

Ward, S. N. (1994). A multidisciplinary approach to seismic hazard in southern California, *Bull. Seism. Soc. Am.* **84,** 1293–1309.

Ward, S. N. (2002). Tsunamis, in *The Encyclopedia of Physical Science and Technology*, R. A. Meyers (Editor), Academic Press, San Diego, 175–191.

Weinstein, S. A., and E. A. Okal (2005). The mantle wave magnitude $M_m$ and the slowness parameter $\Theta$: five years of real-time use in the context of tsunami warning, *Bull. Seism. Soc. Am.* **95,** 779–799.

Wells, D. L., and K. J. Coppersmith (1994). New empirical relationships among magnitude, rupture length, rupture width, rupture area, and surface displacement, *Bull. Seism. Soc. Am.* **84,** 974–1002.

Wessel, P., and W. H. F. Smith (1995). New version of the Generic Mapping Tools released, *EOS Trans. AGU* **76,** F329.

Wu, T. Y. (1981). Long waves in ocean and coastal waters, *J. Eng. Mech. Div. ASCE* **107,** 501–522.

Wyss, M. (1979). Estimating maximum expectable magnitude of earthquake from fault dimensions, *Geology* **6,** 336–340.

Yeh, H., C. Peterson, R. K. Chadha, G. Latha, and T. Katada (2005). The great Sumatra Earthquake and Indian Ocean tsunami of December 26, 2004, Report 2: Tsunami survey along the southeast Indian Coast, EERI Special Earthquake Report, March 2005, 5–8.

Zeng, J. L., T. H. Heaton, and C. DiCaprio (2005). The effect of slip variability on earthquake slip-length scaling, *Geophys. J. Int.* **162,** 841–849.

Zheng, G., and J. R. Rice (1998). Conditions under which velocity-weakening friction allows a self-healing versus a cracklike mode of rupture, *Bull. Seism. Soc. Am.* **88,** 1466–1483.

U.S. Geological Survey
345 Middlefield Road, MS 999
Menlo Park, California 94025
egeist@usgs.gov
(E.L.G., F.F.P.)

National Oceanic and Atmospheric Administration
Pacific Marine Environmental Laboratory
7600 Sand Point Way NE, Bldg. 3
Seattle, Washington 98115
(V.V.T., D.A.)

Joint Institute for the Study of the Atmosphere and Oceans
University of Washington
Seattle, Washington 98195
(V.V.T., D.A.)

New Mexico Tech
Earth and Environmental Science Department
Socorro, New Mexico 87801
(S.L.B.)

Manuscript received 17 January 2006.